Research Paper

PAIN®

OPEN

Mitochondrial calcium uniporter deletion prevents painful diabetic neuropathy by restoring mitochondrial morphology and dynamics

Dale S. George[a], Sandra Hackelberg[a], Nirupa D. Jayaraj[a], Dongjun Ren[b], Seby L. Edassery[a], Craig A. Rathwell[b], Rachel E. Miller[c], Anne-Marie Malfait[c], Jeffrey N. Savas[a], Richard J. Miller[b], Daniela M. Menichella[a,*]

Abstract

Painful diabetic neuropathy (PDN) is an intractable complication affecting 25% of diabetic patients. Painful diabetic neuropathy is characterized by neuropathic pain accompanied by dorsal root ganglion (DRG) nociceptor hyperexcitability, resulting in calcium overload, axonal degeneration, and loss of cutaneous innervation. The molecular pathways underlying these effects are unknown. Using high-throughput and deep-proteome profiling, we found that mitochondrial fission proteins were elevated in DRG neurons from mice with PDN induced by a high-fat diet (HFD). In vivo calcium imaging revealed increased calcium signaling in DRG nociceptors from mice with PDN. Furthermore, using electron microscopy, we showed that mitochondria in DRG nociceptors had fragmented morphology as early as 2 weeks after starting HFD, preceding the onset of mechanical allodynia and small-fiber degeneration. Moreover, preventing calcium entry into the mitochondria, by selectively deleting the mitochondrial calcium uniporter from these neurons, restored normal mitochondrial morphology, prevented axonal degeneration, and reversed mechanical allodynia in the HFD mouse model of PDN. These studies suggest a molecular cascade linking neuropathic pain to axonal degeneration in PDN. In particular, nociceptor hyperexcitability and the associated increased intracellular calcium concentrations could lead to excessive calcium entry into mitochondria mediated by the mitochondrial calcium uniporter, resulting in increased calcium-dependent mitochondrial fission and ultimately contributing to small-fiber degeneration and neuropathic pain in PDN. Hence, we propose that targeting calcium entry into nociceptor mitochondria may represent a promising effective and disease-modifying therapeutic approach for this currently intractable and widespread affliction. Moreover, these results are likely to inform studies of other neurodegenerative disease involving similar underlying events.

Keywords: Painful diabetic neuropathy, Mitochondria, Dorsal root ganglion, Neuropathic pain, Mitochondrial calcium uniporter

1. Introduction

Painful diabetic neuropathy (PDN) is one of the most common and intractable symptoms of diabetes, affecting 25% of patients.[1,2,40,99] Given the increasing prevalence of type II diabetes mellitus,[121] the incidence of PDN is expected to rise.[73] Neuropathic pain associated with PDN is a debilitating affliction with substantial impact on quality of life and healthcare costs.[36] Nonetheless, current therapies for PDN are only partially effective. One critical barrier to developing new treatments for PDN is that the molecular mechanisms leading to neuropathic pain in PDN are still unknown.

The symptoms of PDN include neuropathic pain and small-fiber degeneration,[39,56,76,96] specifically "dying back" or retraction of the axons of small diameter dorsal root ganglion (DRG) nociceptive neurons that innervate the skin.[57] Neuropathic pain is associated with hyperexcitability of neurons in pain pathways in the absence of appropriate stimuli.[56,113,119] The cells responsible for this phenomenon include DRG nociceptors.[56,113,119] Diabetic patients[77] and animal models of PDN[3,14] exhibit sensory neuron hyperexcitability, including the spontaneous activity of DRG nociceptor axons.[3,14,94] Consistent with these findings, our laboratory has recently shown that reducing the hyperexcitability of DRG nociceptors, identified by the sodium channel $Na_v1.8$, which is expressed by 90% of nociceptors,[95] not only reversed mechanical allodynia in the well-established high-fat diet (HFD) mouse model of PDN[76] but also reversed small-fiber degeneration.[51] However, the detailed molecular cascade linking neuropathic pain to axonal degeneration in PDN is not well understood. This gap in knowledge is a critical barrier to developing novel therapeutic approaches for PDN that could not only treat pain but also reverse small-fiber pathology.

Sponsorships or competing interests that may be relevant to content are disclosed at the end of this article.

D.S. George, S. Hackelberg, and N.D. Jayaraj contributed equally to this work.

Departments of [a] Neurology and, [b] Pharmacology, Feinberg School of Medicine, Northwestern University, Chicago, IL, United States, [c] Department of Internal Medicine, Rush Medical College, Chicago, IL, United States

**Corresponding author. Departments of Neurology and Pharmacology, Feinberg School of Medicine, Northwestern University, Robert Lurie Medical Research Center Lurie 8-123, 303 E. Superior St, Chicago, IL 60611, United States. Tel.: 312-503-3223; fax: (312) 503-3202. E-mail address: d-menichella@northwestern.edu (D.M. Menichella).*

Supplemental digital content is available for this article. Direct URL citations appear in the printed text and are provided in the HTML and PDF versions of this article on the journal's Web site (www.painjournalonline.com).

PAIN 163 (2022) 560–578

http://dx.doi.org/10.1097/j.pain.0000000000002391

One phenomenon that could potentially explain both neuropathic pain and small-fiber degeneration is increased excitability and an associated increase in calcium influx into nociceptors, resulting in abnormally high concentrations of intracellular calcium. In support of this idea, hyperexcitability of $Na_v1.8$ DRG neurons was accompanied by increased intracellular calcium concentration ($[Ca^{2+}]_i$) in the HFD mouse model of PDN.[51] Sustained increased $[Ca^{2+}]_i$ is a key component in the signaling pathways leading to axonal degeneration[115] in both the central[33] and peripheral nervous systems.[60,82,109] In particular, increased $[Ca^{2+}]_i$ leads to DRG neurite degeneration in a genetic model of small-fiber neuropathy.[43] Thus, our goal in this study was to understand how diabetes, hyperexcitability, and increased $[Ca^{2+}]_i$ in $Na_v1.8$ DRG neurons are causally connected to axonal degeneration and pain.

One way that increased $[Ca^{2+}]_i$ might contribute to axonal damage is through alteration of mitochondrial function,[12] including alteration of mitochondrial calcium homeostasis.[87] Calcium signaling can also affect mitochondrial morphology and dynamics by regulating dynamin-related protein 1 (Drp1) phosphorylation.[19,35,48] Mitochondria have been implicated in the pathology of PDN.[110,111] DRG neurons from animal models of type II diabetes show downregulation of mitochondrial respiratory chain complex proteins[89] and reduced respiratory chain activity.[30] Furthermore, mitochondrial morphology and localization are altered in rodent models of PDN and in patients with PDN.[29,41,59,110,111] In a genetic model of type-2 diabetes, the db/db mouse, DRG neurons showed elevated calcium levels[50] and altered mitochondrial calcium homeostasis,[44] as well as altered mitochondrial morphology, including small and fragmented mitochondria,[41] increased fission,[41] and changes in mitochondrial trafficking.[90]

Appropriate mitochondrial dynamics and morphology are vital for neuronal function.[21,34] Mitochondrial dynamics describe ongoing changes in intermitochondrial networks, as well as mitochondrial shape, size, connectivity, trafficking, and activity.[21] Mitochondrial morphology, which can range from an interconnected reticulum to fragmented puncta, is determined by the balance between the opposing forces of fusion and fission (reviewed in Ref. 92). A critical role has been proposed for intramitochondrial $[Ca^{2+}]_i$ in the regulation of mitochondrial dynamics and morphology.[19,35,48] One major pathway for mitochondrial calcium influx is through the mitochondrial calcium uniporter (MCU), a selective calcium channel that facilitates transport of calcium across the inner mitochondrial membrane when intracellular calcium concentration $[Ca^{2+}]_i$ rises above the "set point."[9,37] Mitochondrial calcium uniporter expression is upregulated in other scenarios of calcium overload, such as myocardial ischemia or reperfusion (I/R) injury,[120] and mitochondrial fission is enhanced.[47,120] In I/R injury, blocking the MCU pharmacologically reduces myocardial infarction by alleviating mitochondria fission.[120] Whether there are similar mechanisms at play in the pathogenesis of axonal degeneration and mechanical allodynia in PDN is unknown.

Using the well-established HFD mouse model of PDN,[76] we now demonstrate that mitochondrial proteins are differentially expressed (DE) in DRG neurons, including elevated levels of mitochondrial proteins involved in fission. Furthermore, using electron microscopy (EM), we show that mitochondria in DRG nociceptors have fragmented morphology as early as 2 weeks after starting HFD, preceding the onset of mechanical allodynia and small-fiber degeneration. Moreover, preventing calcium entry into the mitochondria by selectively deleting the MCU from nociceptors restored normal mitochondria morphology and dynamics, prevented axonal degeneration, and reversed mechanical allodynia in the HFD mouse model of PDN. Hence, we propose that targeting MCU-mediated increases in calcium influx into nociceptor mitochondria may be a promising approach to disease-modifying treatments for patients suffering from PDN.

2. Materials and methods

2.1. Animals

All methods involving animals were approved by the Institutional Animal Care and Use Committee at Northwestern University. Animals were housed with food and water ad libitum on a 12-hour light cycle. We used the following mouse lines: C57/Bl6J (wild-type), $Na_v1.8$-Cre mice kind gift from Dr. John Wood[100] $Na_v1.8$-Cre; Ai9 mice, $Na_v1.8$-Cre; GCaMP6s, MCU-floxed mice ($MCU^{flox/flox}$) kind gift from Jeffery Molkentin,[54] $Na_v1.8$-Cre; Ai9; $MCU^{fl/+}$ (Het), $Na_v1.8$-Cre; Ai9; and $MCU^{fl/fl}$ (Homo).

2.2. High-fat diet

High-fat diet is a common rodent model of type-II diabetes.[76] Mice were fed 42% fat (Envigo TD88137, Indianapolis, IN) for 10 weeks. Control mice were fed a regular diet (RD) (11% fat). After 10 weeks on RD or HFD, a glucose tolerance test was performed as described.[51,76] In brief, after fasting for 12 hours, mice were injected with a 45% D-glucose solution (2 mg glucose/g body weight). Animals were weighed on an electronic scale, and after fasting for 12 hours, the animals' fasting blood glucose was measured using TRUEtrack meter and TRUEtrack glucose test strips. The mice were then injected with a 45% D-glucose solution (2 mg glucose/g body weight), and blood glucose was measured at 30, 60, and 120 minutes after injection (RD-Het n = 12, RD-Homo n = 6, HFD-Het n = 15, and HFD-Homo n = 15). To compare "diabetic" vs "nondiabetic" HFD mice, we set the cutoff for diabetes (>140 mg/dL) at 2 SDs above the mean for glucose at 2 hours after glucose challenge, as determined from among wild-type littermate RD mice.[51]

2.2.1. Statistics

The area under the curve (AUC) was calculated for all time points in GraphPad Prism 8.3, and the mean total peak area was calculated for each animal. Blood glucose and AUC were analyzed using 1-way analysis of variance (ANOVA) followed by the Tukey test.

2.3. Preparation of dorsal root ganglion extracts for tandem mass tag–based quantitation

Lumbar DRG (L1-L6) from 8 RD and 8 HFD mice were extracted and flash frozen. The DRG tissue extracts were homogenized in 150 μL radioimmunoprecipation assay buffer (RIPA) (0.1% SDS, 1% NP40, and 0.5% sodium deoxycholate) containing protease inhibitors. Next, they were sonicated 3 times for 5 seconds (amplitude = 25%) and incubated in ice for 15 minutes. Proteins were precipitated with methanol–chloroform before resuspension in 6M guanidine in 100 mM triethylammonium bicarbonate (TEAB). Disulfide bonds were reduced with dithiothreitol (DTT), and cysteine residues were alkylated with iodoacetamide. Proteins were then digested for 3 hours with 2 μg of endoproteinase LysC (Promega Cat# VA1170) and subsequently digested overnight with 2 μg of trypsin (Promega V5280). The digest was then acidified with formic acid to a pH of ~2 to 4 and

desalted by using C18 HyperSep Cartridges (cat# 60108-302; Thermo Scientific, Rockford, IL). The eluted peptide solution was completely dried before buffer change and measuring their concentration by micro bicinchoninic acid assay (BCA) assay (Thermo Scientific). An equal quantity of peptides (~100 μg) from each sample was then used for isobaric labeling. Tandem mass tag (TMT)-16 plex peptide labeling was performed according to the manufacturer's instructions (Thermo Scientific cat# A44521). After 2 hours incubation at room temperature, the reaction was quenched with hydroxylamine at a final concentration of 0.3% (vol/vol). Isobaric labeled samples were then combined 1:1:1:1:1:1:1:1:1:1:1:1:1:1:1:1 and lyophilized. The pooled labeled peptides were fractionated into 8 fractions using the high pH fractionation kit (Thermo Scientific cat# 84868). Fractionated samples concentration was again determined by micro BCA. Peptide solutions were dried, stored at −80°C, and reconstituted in liquid chromatography - mass spectrometry (LC-MS) buffer A (5% acetonitrile and 0.125% formic acid) until liquid chromatography with tandem mass spectrometry (LC-MS) analysis.

2.4. Nanoflow LC with MultiNotch MS2/MS3 Orbitrap Fusion MS analysis

Three micrograms from each fraction were loaded for LC-MS analysis using a Thermo Orbitrap Fusion coupled to a Thermo EASY nLC-1200 UPLC pump and vented Acclaim PepMap 100, 75 μm × 2 cm nanoViper trap column and nanoViper analytical column (Thermo—164570), 3 μm, 100Å, C18, 0.075 mm, 500 mm with stainless steel emitter tip assembled on the Nanospray Flex ion source with a spray voltage of 2000 V. The chromatographic run was performed by 4 hours gradient beginning with 100% buffer A (5% acetonitrile and 0.125% formic acid), 0% B (95% acetonitrile and 0.125% formic acid), and increased to 7% B over 5 minutes, then to 25% B over 160 minutes, 36% B over 40 minutes, 45% B over 10 minutes, 95% B over 10 minutes, and held at 95% B for 15 minutes before terminating the scan. The MultiNotch MS3 method[70] was programmed as per the following parameters: ion transfer tube temp = 300°C, Easy-IC internal mass calibration, default charge state = 2, and cycle time = 3 seconds. MS1 detector was set to Orbitrap with 60 K resolution, wide quad isolation, mass range = normal, scan range = 300 to 1800 m/z, max injection time = 50 ms, automatic gain control (AGC) target = 2×10^5, microscans = 1, R- focus lens (RF) = 60%, without source fragmentation, and data type = positive and centroid. Monoisotopic precursor selection was set to include charge states 2 to 7 and reject unassigned. Dynamic exclusion was allowed, n = 1 exclusion for 60 seconds with 10 ppm tolerance for high and low. An intensity threshold was set to 5×10^3. Precursor selection decision = most intense, top speed, 3 seconds. MS2 settings include isolation window = 0.7, scan range = auto normal, collision energy = 35% collision induced disassociation (CID), scan rate = turbo, max injection time = 50 ms, AGC target = 1×10^4, and Q = 0.25. In MS3, the top 10 precursor peptides selected for analysis were then fragmented using 65% HCD before Orbitrap detection. A precursor selection range of 400 to 1200 m/z was chosen with mass range tolerance. An exclusion mass width was set to 18 p.p.m. on the low and 5 p.p.m. on the high. Isobaric tag loss exclusion was set to TMT reagent. Additional MS3 settings include an isolation window = 2, Orbitrap resolution = 60 K, scan range = 120 to 500 m/z, AGC target = 1×10^4, max injection time = 120 ms, microscans = 1, and data type = profile.

2.4.1. Analysis of tandem mass spectra

The Integrated Proteomics Pipeline—IP2—(Integrated Proteomics Applications, Inc, San Diego, CA www.integratedproteomics.com/) was used to analyze the proteomic results with ProLuCID, DTASelect2, Census, and QuantCompare. The raw spectral raw files were extracted into MS1, MS2, and MS3 files using the in-house program RawConverter.[49] Spectral files were then pooled from fractions for each sample and searched against the UniProt mouse protein database and matched to sequences using the ProLuCID or SEQUEST algorithm (ProLuCID ver. 3.1) with 50 p.p.m. peptide mass tolerance for precursor ions and 600 p.p.m. for fragment ions. Fully and half-tryptic peptide candidates were included in search space, all that fell within the mass tolerance window with no miscleavage constraint and assembled and filtered with DTASelect2 (ver. 2.1.3) through the Integrated Proteomics Pipeline (IP2 v.5.0.1, Integrated Proteomics Applications, Inc). Static modifications at 57.02146 C and 229.162932 K and N-term were included. The target-decoy strategy was used to verify peptide probabilities and false discovery ratios.[42] Minimum peptide length of 5 was set for the process of each protein identification. Each data set had an 1% false-discovery rate at the protein level based on the target-decoy strategy. Isobaric labeling analysis was performed with Census 2 as previously described.[80] Tandem mass tag channels were normalized by dividing each by the sum of all channels. No intensity threshold was applied.

2.4.2. Heat maps, clustering, and volcano plots for the recovery period

Reporter ion intensity from the MS/MS analysis was analyzed using NCI-BRB Array Tool software (BRB-ArrayTools Version: 4.6.1—Stable, R version 3.6.2) The data were normalized using quantile normalization, and differentially expressed (DE) proteins were selected based on the univariate *t* test with a Benjamini Hochberg adjusted *P*-value cutoff 0.05.

2.5. Electron microscopy methods

For EM, L4 and L5 lumbar DRG were extracted and fixed in 2.5% glutaraldehyde in 0.1M sodium cacodylate buffer pH 7.3 and postfixed with 2% osmium tetroxide in unbuffered aqueous solution, rinsed with distilled water, en bloc stained with 3% uranyl acetate, rinsed with distilled water, dehydrated in ascending grades of ethanol, transitioned with propylene oxide, embedded in resin mixture of Embed 812 kit, and cured in a 60°C oven. Samples were sectioned on a Leica Ultracut UC6 ultramicrotome. 1-μm thick sections were collected and stained with Toluidine Blue O, and 70 nm sections were collected on 200 mesh copper grids; thin sections were stained with uranyl acetate and Reynolds lead citrate. Samples were imaged using a field electron and ion company (FEI) Tecnai Spirit G2 transmission electron microscope (FEI) operated at 80 kV. Images were captured with an Eagle 4k HR 200 kV CCD camera.

2.5.1. Image analysis

To determine the neuronal size, the sections were first imaged at a low magnification (×690). Once small–medium diameter neurons were identified (<40 μm), images were acquired at ×9300. The electron micrographs were analyzed using Fiji (national institute of health (NIH)). The boundary for each mitochondrion was manually marked using the free-hand selection tool, and the area and perimeter for each mitochondrion

were measured. Interconnectivity was measured by dividing the area by the perimeter. Interconnectivity is a measure or an indicator of fragmentation, with a lower score indicating a more fragmented state. Other parameters measured include circularity, aspect ratio, and form factor, as described by Picard et al., 2013.

2.5.2. Statistics

The data did not have a normal distribution as determined by the D'Agostino and Pearson omnibus normality test (WT DRG n = 60 mitochondria for 2 weeks and 10 weeks RD and HFD, WT Remak bundle n = 40 mitochondria for 10 weeks RD and HFD, and MCU n = 120 mitochondria for all conditions). Thus, data were analyzed by a nonparametric (Kruskal–Wallis) 1-way ANOVA followed by the Dunn multiple comparison test. Data are reported as median ± SEM.

2.6. In vitro calcium imaging

$Na_v1.8$-Cre; Ai9 mice fed either a RD or HFD for 10 weeks were used for these experiments. In brief, DRG primary cultures were prepared as described previously,[51] and the neurons were grown on 15 mm coverslips. The cultures were incubated in calcium imaging buffer (140 mM NaCl, 10 mM Hepes, 2 mM $CaCl_2$, 1 mM $MgCl_2$. $6H_2O$, 10 mM glucose, and 2.5 mM KCl), with 5 μM Fura-2 acetoxymethyl (AM) ester (Thermo Fisher Scientific) at 37°C in the dark for 30 minutes and placed into dye free solution for an additional 30 minutes. For imaging, cover slips were fastened in the recording chamber and bathed in extracellular solution with a flow rate of 2 mL/minute. Time lapse recordings were acquired with an Olympus IX70 inverted epifluorescence microscope with a 20x (0.7 NA) air objective at 3 seconds intervals with 340 and 380 nm excitation and 510 nm emission at RT. Fluorescence was monitored with regions of interest (ROI) at the soma. Bath flow was stopped, and baseline fluorescence was recorded for 2 minutes. For identification of $Na_v1.8$ positive neurons, fluorescence images were taken with unfiltered excitation and 615 nm emission. TIFF images were exported to Fiji (NIH) and final ROI in the cytoplasm selected. Intensity data and area were imported to Igor Pro (Wave Metrics) and analyzed using custom procedures. In brief, intensity measures were background subtracted, and the ratio of fluorescence at 340 and 380 nm was calculated (263 neurons from n = 3 animals and 241 neurons from n = 3 animals were measured in RD and HFD, respectively).

2.6.1. Statistical analysis

Normalized fluorescence values were tested for statistical significance by unpaired *t* tests.

2.7. In vivo calcium imaging

Animals were fed an RD or HFD diet for 10 weeks, then anesthetized by isoflurane, and laminectomized, exposing the L4 DRG as described.[74] The experimental set-up and imaging were performed as previously reported.[74] In brief, the mouse was positioned under the microscope by clamping the spinal column at L2 and L6; body temperature and isoflurane were constantly maintained and monitored throughout the imaging period. Silicone elastomer (World Precision Instruments, Sarasota, FL) was used to cover the exposed DRG and surrounding tissue to avoid drying.[74] A Coherent Chameleon-Ultra2 Ti:Sapphire laser was tuned to 920 nm, and GCaMP6s signal was collected by using a bandpass filter for the green channel (490-560 nm). Image acquisition was controlled using PrairieView software version 5.3. Images of the L4 DRG were acquired at 0.7 Hz, with a dwell time of 4 μs/pixel (pixel size 1.92 × 1.92 μm^2) and a 10x air lens (Olympus UPLFLN U Plan Fluorite, 0.3 NA, 10 mm working distance). The scanned sample region was 981.36 x 981.36 μm^2. Anesthesia was maintained using isoflurane (1.5%-2%) during imaging. Images were acquired for 30 frames. A 200 to 250 g force (referred to as the quantitative mechanical force (QMF)) was applied to the hind paw for each mouse (RD n = 7, HFD n = 10) from frame 10 through 20 using a calibrated forceps system.

2.7.1. Intradermal capsaicin administration

Five microliter of 10 mM capsaicin was injected intradermally to the paw pad in the hind paw of anesthetized mice in the set up described in the previous section. The needle was inserted into the paw from frame 20 to 25, and any responses to the needle were not included in the analysis. After 25 frames, capsaicin was released and the neurons that responded to capsaicin and QMF were counted and reported as the percentage of QMF (100%) that responded to capsaicin as well (n = 3 for RD and HFD).

2.7.2. Analysis of in vivo calcium imaging

Time series files were exported and further processed in Fiji (NIH). Any movement in the time series (on account of breathing) was adjusted using the template-matching plugin. Brightness and contrast were adjusted, and cells (region of interest, ROI) were identified by looking for an increase in fluorescence during the stimulus application period, as previously reported.[74] The identified cells were then carefully marked, and a custom macro (where changes in $[Ca^{2+}]_i$ were quantified by calculating the change in fluorescence for each ROI in each frame t of a time series using the formula: $\Delta F/F_0 = (F_t - F_0)/F_0$, where F_o = the average intensity during the baseline period prior to the application of the stimulus) was run followed by a Multi Measure Plugin to obtain the mean gray value of each ROI. Once the values were obtained, the ROIs that had a fluorescence reading 6 × SD to the baseline (t = 0-9 frames) were included as a responding ROI/neuron (n = 7 RD, n = 10 HFD). If there were no responses to the stimulus, the animal was excluded from the analysis; based on this predetermined criterion, one RD animal was excluded from the analysis. To determine the percentage of responders, the total number of neurons imaged for each DRG was estimated by counting the number of neurons within a region of average density and extrapolating to the total DRG area.[74] The AUC was calculated for each responding ROI in GraphPad Prism 8.3, and the mean total peak area was calculated for each animal. The maximum amplitude was calculated by taking the maximum $\Delta F/F_0$ value for each responding ROI, and the mean was calculated for each animal. In addition, to focus on the subpopulation of neurons with high-intensity responses to QMF, a second set of analyses focused on identifying responding ROIs as those neurons that showed a $\Delta F/F_0 > 2$, and again the percentage of responders, mean total peak area, and mean max fluorescence were calculated for each animal. To measure the neuronal area, the ROIs that responded to the QMF were marked and the area was measured in Fiji.

2.7.3. Statistical analysis

Percentage responders, AUC, and max amplitude were compared using a 2-tailed unpaired *t* test. Data were reported as mean ± SD.

2.8. Detection of cutaneous innervation

Animals were fed a RD or HFD for 10 weeks. The hind paws were harvested and fixed in 4% paraformaldehyde (PFA) for 24 hours, and then the overlying footpad skin was dissected, submerged in 30% sucrose solution for 24 hours, and embedded in the optimal cutting temperature compound (OCT, Tissue-Tek, Torrence, CA). 20 μm sections were cut on a cryostat and counterstained by mounting solution with 4'6-diamidino-2-phenylindole (Hard-Set, Vectashield).

2.8.1. Confocal analysis

Two to 3 separate sections from each animal were analyzed, and 3 separate composite Z-stack images of skin from the hind paw were imaged using Olympus FV10i, and the images were processed using Fiji. The epidermal–dermal junction was outlined by a blinded observer who also noted its length. Two blinded reviewers counted the nerves crossing this line using the Cell Counter plugin. The mean values of the counts from blinded reviewers were divided by the epidermal–dermal junction length to report intraepidermal nerve fiber (IENF) density.

2.8.2. Statistical analysis

Data were compared using 1-way ANOVA followed by the Tukey test. In all experiments (RD-Het n = 3, RD-Homo n = 3, HFD-Het n = 5, and HFD-Homo n = 5), values are expressed as mean ± SD.

2.9. Immunohistochemical labeling of the dorsal root ganglion

Adult mice were deeply anesthetized with isoflurane, laminectomy was performed, and DRGs (lumbar L3-L5) were extracted and fixed in 4% PFA for 24 hours. The samples were then transferred to 30% sucrose for 24 hours and embedded in OCT. Sections (20 μm) were cut on a cryostat and counterstained with I-isolectin B4 (IB4 isolectin GS-IB4 Alexa Fluor 647 conjugate) (Invitrogen, Thermo Fisher Scientific, Waltham, MA, catalog I32450, 1:100). Tissue sections were analyzed by confocal microscopy (RD-Het n = 3, RD-Homo n = 4, HFD-Het n = 4, and HFD-Homo n = 4).

2.9.1. Statistical analysis

Data were analyzed using 1-way ANOVA followed by the Tukey multiple comparison test. Data were reported as mean ± SD.

2.10. RNAscope in situ hybridization

RNAscope in situ hybridization multiplex V2 was performed according to the manufacturer's instructions (Advanced Cell Diagnostics, Newark, CA). Dorsal root ganglia were isolated in an RNase free manner, and the samples were then fixed in RNase free 4% PFA for 24 hours. The samples were then transferred to 30% sucrose for 24 hours and embedded in OCT. 20 μm sections were placed on Superfrost Plus charged slides and stored at −20°C until ready to use. The slides were briefly washed in 1× phosphate buffered saline (PBS) and followed by a 10-minute hydrogen peroxidase treatment at RT. The slides were then placed in a beaker containing 1× target retrieval solution, which was heated to around 99 to 102°C for about 3 minutes. The slides were then cooled in DEPC-treated water and transferred to 100% ethanol for 3 minutes. The slides were allowed to completely air dry, and hydrophobic barriers were drawn around the sections. The air-dried slides were placed on the HybEZ slide rack, and about 5 drops of RNAscope Protease III was added. The slide rack was placed onto a prewarmed humidity control tray and into the HybEZ oven at 40°C for 30 minutes. Probes Scn10a/$Na_v1.8$ (C1, catalog 426011), NF200 (C2, catalog 443671-C2), and Calca/CGRP (C2, catalog 578771-C2) were used at the recommended concentration (C1:C2; 50:1). Probes were incubated for 2 hours at 40°C, and the slides were then stored in 5X saline sodium citrate solution. On day 2, AMP1, AMP2, and AMP3 were added sequentially with a 30-minute, 30-minute, and 15-minute incubation period, respectively. Depending on the probe used, the appropriate HRP signals were developed. In brief, 4 to 6 drops of HRP-C1 or HRP-C2 were added and incubated for 15 minutes at 40°C. This was followed by the addition of 1:100 dilution of TSA Plus fluorescein. The fluorophores were incubated at 40°C for 30 minutes, followed by addition of the HRP blocker. Washes were performed using 1X wash buffer as recommended. The slides were then mounted using VECTASHIELD antifade mounting media containing DAPI. Tissue sections were analyzed by imaging the whole DRG using confocal microscopy (all conditions had an n = 3 animals).

2.10.1. Statistical analysis

Data were analyzed using an ordinary 1-way ANOVA followed by the Tukey multiple comparison test. Data were reported as mean ± SD.

2.11. von Frey

von Frey behavioral studies were performed as described. In brief, mice were placed on a metal mesh floor and covered with a transparent plastic dome where they rested quietly after an initial few minutes of exploration. Animals were habituated to this apparatus for 30 minutes a day and 2 days before behavioral testing. After acclimation, each filament was applied to 6 spots spaced across the glabrous side of the hind paw. Mechanical stimuli were applied with 7 filaments, each differing in the bending force delivered (10, 20, 40, 60, 80, 100, and 120 mN), but each fitting a flat tip and a fixed diameter of 0.2 mm. The force equivalence is 100 mN = 10.197 g. The filaments were tested in order of ascending force, with each filament delivered for 1 second in sequence from the first to the sixth spot, alternately from one paw to the other. The interstimulus interval was 10 to 15 seconds.[51] The von Frey withdrawal threshold was defined as the force that evoked a minimum detectable withdrawal on 50% of the tests at the same force. Experimental procedures were designed to maximize robustness and minimize bias. Specifically, von Frey experiments were conducted using random experimental group assignments (diet and treatment). Investigators who performed von Frey tests and endpoint analysis were blinded to the experimental conditions. We have experience with randomized allocation and blinded analysis using this mouse model with sequenced numbering of mice at weaning.[51]

2.11.1. Statistical analysis

The incidence of foot withdrawal was expressed as a percentage of 6 applications of each filament as a function of force. The Hill equation was fitted to the function (Origin version 6.0, Microcal Software), relating the percentage of indentations eliciting a withdrawal to the force of indentation. From this equation, the threshold force was defined as the force corresponding to a 50%

withdrawal rate.[51] Data were compared by 1-way ANOVA followed by the Tukey test (RD-Het n = 8, RD-Homo n = 6, HFD-Het n = 12, and HFD-Homo n = 15) and reported as mean ± SD.

2.12. Hargreaves method

The mice were habituated in a testing room for 30 minutes a day, for 2 trial days and on the test day. After acclimatization, animals were compartmentalized into its own enclosure. An infrared emitter at an intensity of 55[27] was positioned underneath the center of the hind paw. The timer starts automatically when the infrared beam is turned on, and the timer ends when the animal withdraws the paw. The reaction time is recorded only when the animal showed nocifensive behavior such as flicking, biting, shaking, or kept the paw raised for a brief time >2 seconds. The infrared beam is cutoff automatically if the animal did not respond within 20 seconds. The test is repeated 5 times to obtain an average reaction time per animal, and a 5-minute interval is given before the test is repeated on the same animal.[23]

2.12.1. Statistical analysis

Data were compared using 1-way ANOVA followed by the Tukey test (RD-Het n = 6, RD-Homo n = 5, HFD-Het n = 5, and HFD-Homo n = 7) and reported as mean ± SD.

2.13. Paw hyperalgesia

Paw hyperalgesia was measured in $Na_v1.8$-Cre; Ai9 mice (n = 12 per condition) using a Pressure Application Measurement (PAM) device (Ugo Basile, Germany) as previously described.[74] In brief, mice were restrained by hand, and the PAM transducer was pressed against the hind paw of the animals. The experimenter used the PAM software as a guide to apply an increasing amount of constant force, up to a maximum of 450 g. The force at which the animal tried to withdraw the paw was noted as the withdrawal threshold. Two measurements per paw were averaged to report the withdrawal threshold.

2.13.1. Statistical analysis

Data were compared using an unpaired *t* test.

3. Results

3.1. Mitochondrial proteins are differentially expressed in dorsal root ganglion neurons of diabetic mice

We used an unbiased approach to elucidate the molecular mechanisms that underlie neuropathic pain and axonal degeneration in the HFD mouse model of PDN. Using 16 plex TMT quantitative proteomic analysis of lumbar DRG extracts from mice fed a RD or an HFD for 10 weeks (**Fig. 1**), we identified 5249 proteins in each data set of 8 biological replicates from each group. We identified 1121 unique proteins (false discovery rate < 0.05) that were DE between RD and HFD (**Fig. 1A**). Of these, about 14% were associated with mitochondria, according to the Mouse MitoCarta 2.0 database[18] (**Fig. 1B**). A Gene Ontology analysis of DE mitochondrial proteins indicated several significantly enriched pathways, including mitochondrial organization and mitochondrial calcium ion transmembrane transport (**Fig. 1C**). Mitochondrial fission 1 protein (Fis1) and mitochondria calcium uniporter regulator 1 (MCUR1) were among the top 10 most elevated mitochondrial proteins in HFD mice compared with RD mice (**Fig. 1D**). Using the MGI Gene Ontology database,[16] we determined the status of proteins involved in fission in our proteomic data set (**Fig. 1E**). Several proteins showed no significant difference. However, we found that several mitochondrial proteins, including Drp1 (also referred to as dynamin-1 like protein), mitochondrial fission 1 protein (Fis1), and mitochondrial fission factor (Mff), were elevated in lumbar DRGs from mice fed a HFD compared with mice fed a RD (**Figs. 1E and F**). Fis1 and Mff are receptors that recruit the Drp1 to mitochondria. Mff is a GTP-hydrolyzing mechanoenzyme that catalyzes mitochondrial fission in the cell, whereas Fis1 plays a minor role in Drp1 recruitment.[64,78] Mff is an outer mitochondrial membrane protein that binds to the GTPase Drp1 to form a complex that promotes mitochondrial fission. Mff overexpression causes mitochondrial fragmentation, consistent with increased fission rates.[64,78] These data suggest a role for mitochondria in the pathogenesis of axonal degeneration and mechanical allodynia in the HFD mouse model of PDN. In particular, the fact that proteins involved in promoting fission were elevated suggests that excessive fission and fragmented mitochondria morphology could underlie axonal degeneration in PDN.

3.2. Altered calcium signals in $Na_v1.8$-positive dorsal root ganglion neurons from diabetic mice

We previously showed that hyperexcitability in $Na_v1.8$-expressing DRG neurons was accompanied by increased $[Ca^{2+}]_i$ ex vivo, in acutely isolated DRG explants from mice fed a HFD, as compared with those fed a RD.[51] Here, we asked whether increased $[Ca^{2+}]_i$ occurs in $Na_v1.8$-expressing DRG neurons in diabetic animals in vivo. To identify differences in the sensitivity of neurons to mechanical stimuli, we used a nonnoxious mechanical stimulus by applying a QMF to the hind paw while recording in vivo calcium as a readout (**Fig. 2A**). To determine the force that can be categorized as nonnoxious in awake behaving mice, we measured paw hyperalgesia in mice fed a RD or HFD at 10 weeks. We determined that a force of 422.8 ± 18.52 g and 380.7 ± 53.19 (Suppl Fig. 1A, available at http://links.lww.com/PAIN/B424) was noxious in RD and HFD, respectively. We therefore chose a force below this withdrawal threshold at 200 to 250 g as the nonnoxious mechanical stimulus. We performed additional in vitro Fura-2 calcium imaging experiments using acutely dissociated $Na_v1.8$ DRG neurons from mice fed a RD or HFD and found no differences in the absolute baseline (F0) calcium levels (Suppl Fig. 1B, available at http://links.lww.com/PAIN/B424; RD 0.65 ± 0.24; HFD 0.61 ± 0.11, $P = 0.84$), suggesting that the baseline calcium is not affected by diet.

Given the cellular diversity and functional heterogeneity of DRG neurons,[26,45,61,108] we selectively monitored $[Ca^{2+}]_i$ in vivo in $Na_v1.8$-positive DRG nociceptors by expressing the $[Ca^{2+}]_i$ indicator protein GCaMP6[24] in these neurons ($Na_v1.8$-Cre mice[100] crossed with conditional reporter GCaMP6 mice; $Ai96^{flox/flox}$; RCL-GCaMP6s).[24] Mice were then fed either a RD or HFD for 10 weeks. Laminectomy was performed on anesthetized mice to expose the fourth lumbar (L4) DRG, which contains sensory neurons that innervate the paw.[74] We applied to the mouse paw a calibrated forceps to deliver a 200 to 250 g force, and real-time neuronal responses to the stimulus were recorded and compared (**Figs. 2B–E**; and supplemental video 1, 2, available at http://links.lww.com/PAIN/B425 and http://links.lww.com/PAIN/B426). The number and percentage of responding neurons along with the intensity of the response was assessed; representative images are shown in **Figure 2b**. We found an increase in the percentage of neurons that responded to

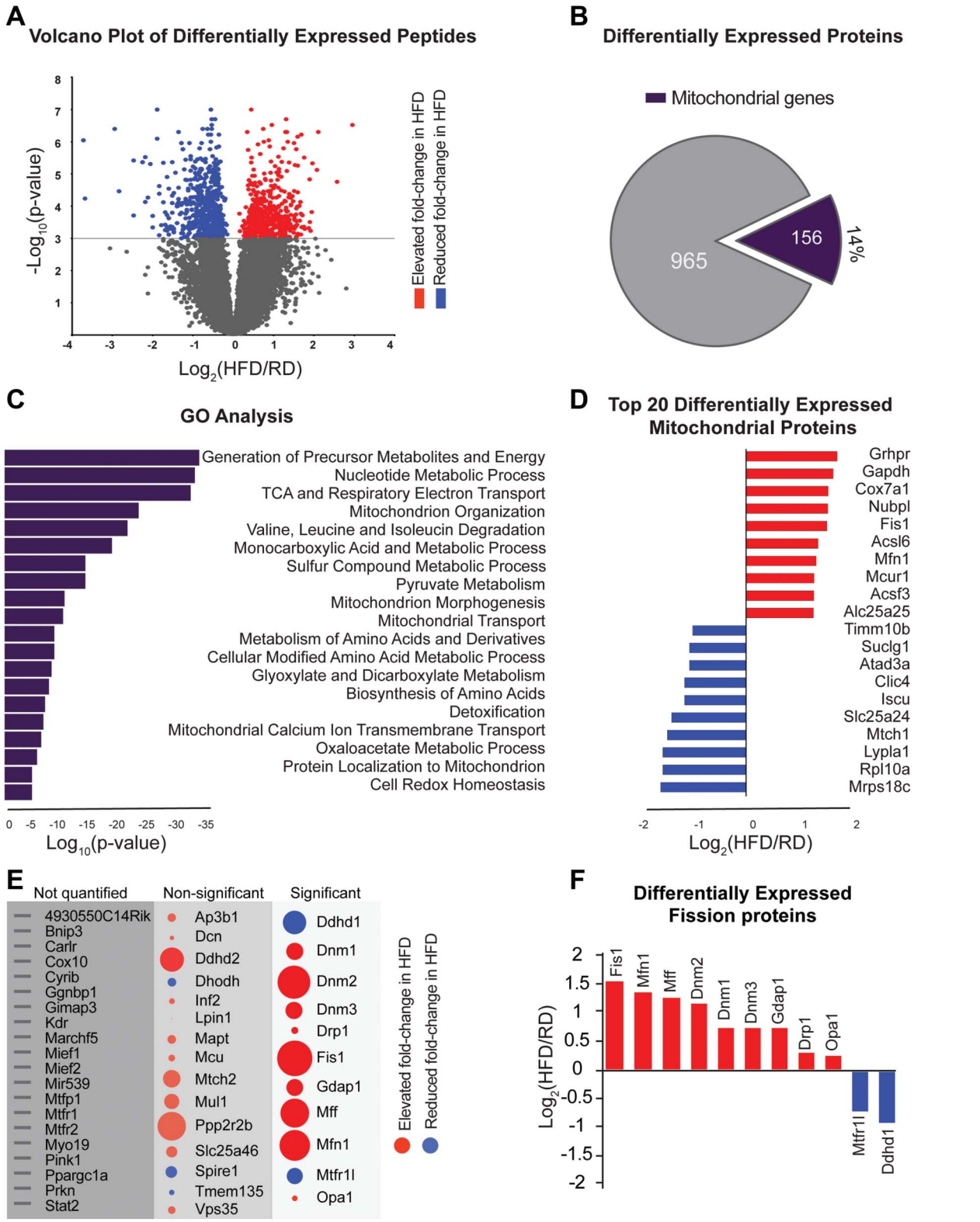

Figure 1. Discovery-based quantitative proteomic analyses of lumbar L4 DRG extracts from mice fed a RD or HFD. (A) Volcano plot showing differentially expressed proteins [FDR < 0.05] between RD and HFD groups. (B) Mitochondrial proteins comprise about 14% of the differentially expressed proteins. (C) The list of differentially expressed mitochondrial proteins passed through a Gene ontology Analysis showing the enriched pathways. (D) Top 10 most elevated (red) and the most decreased (blue) mitochondrial proteins, listed in order of fold change. (E) List of mitochondrial fission proteins classified based on whether it was identified, nonsignificant, or significant. (F) Differentially expressed mitochondrial fission proteins listed in order of fold change. DRG, dorsal root ganglion; FDR, false discovery rate; HFD, high-fat diet; RD, regular diet.

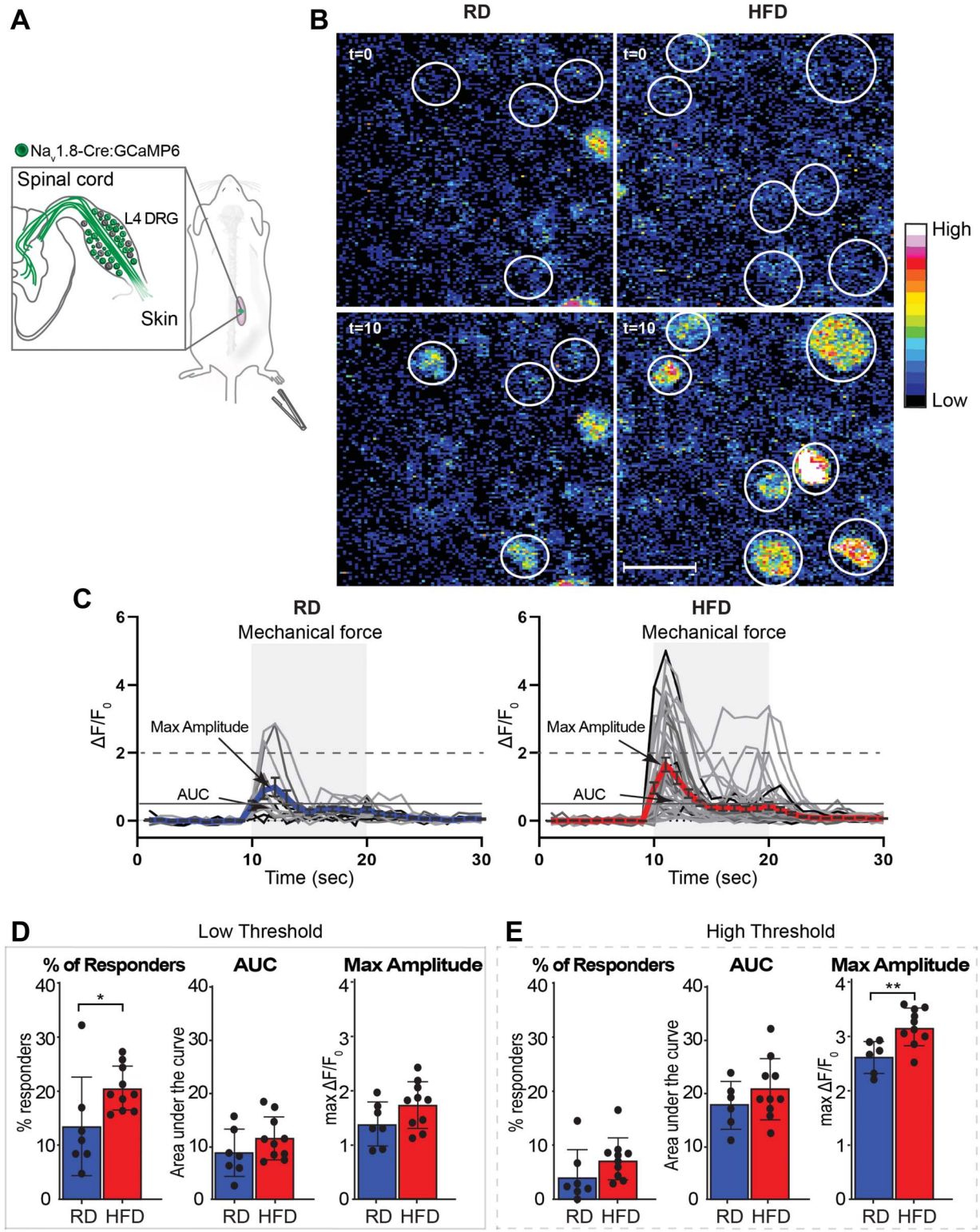

Figure 2. Increased percentage and amplitude of calcium responses in Na$_v$1.8-expressing DRG neurons from mice fed a HFD. (A) Illustration of in vivo calcium imaging setup using Na$_v$1.8-Cre: GCamp6 mice. (B) Representative images taken from RD (left) and HFD (right) mice showing neurons identified by circles at t = 0 seconds (baseline) and t = 10 seconds (QMF of 200-250 g). A 16-color scale is used to emphasize the intensity or amplitude of $[Ca^{2+}]_i$ response. Scale bar represents 50μm. (C) All responses from representative RD and HFD mice (one from each group). The blue (RD) or red (HFD) trace indicates the average change in fluorescence intensity over time. The horizontal solid gray line shows the 6xSD cutoff used to determine a response. The horizontal dashed gray line indicates cutoff of $\Delta F/F_o > 2$. (D) Graphs showing percentage of neurons responding to a QMF of 200 to 250 g applied to the paw, AUC, and maximum amplitude of the calcium transients with a cutoff of 6xSD. Each black dot represents one animal. (E) Graphs showing percentage of neurons, AUC, and maximum amplitude of the calcium transients with a cutoff of $\Delta F/F_o > 2$ between RD and HFD. $^*P < 0.05$, $^{**}P < 0.01$. AUC, area under the curve; DRG, dorsal root ganglion; HFD, high-fat diet; RD, regular diet; QMF, quantitative mechanical force.

the stimulus in HFD (**Figs. 2B and D**; RD 13.48 ± 9.1; HFD 20.44 ± 4.12, $P = 0.04$, circles identify the responding neurons) indicating that additional neurons now have been recruited to respond to this force, that is, were sensitized. **Figure 2C** shows the traces (change in fluorescence with time [$\Delta F/F_0$]) of individual responding neurons (gray line indicates the cutoff for response) from the RD and HFD groups (**Fig. 2C**). The duration of the response, measured by AUC, suggested no difference between RD (8.78 ± 4.42) and HFD (11.60 ± 4.03, $P = 0.19$; **Fig. 2D**). Focusing on the $Na_v1.8$-positive DRG neurons responding to a nonnoxious mechanical stimulus or QMF, we further determined their neuronal size distribution (Suppl Fig. 1c, available at http://links.lww.com/PAIN/B424) and their response to capsaicin (Suppl Fig. 1d, available at http://links.lww.com/PAIN/B424) and found no statistically significant difference when comparing RD and HFD groups.

Among the HFD group, a large number of responses were similar in amplitude to those seen in RD (**Fig. 2C**, blue and the red traces indicate the average of response from RD and HFD, respectively, RD, 1.39 ± 0.40; HFD 1.74 ± 0.43, $P = 0.11$). However, there was also a population of neurons from the HFD group that had a higher amplitude of response. To capture this subset of neurons, we used a higher cutoff threshold (2x change in fluorescence, dashed gray line). Among the population of neurons meeting this criterion (**Fig. 2C**, dashed gray lines), the maximum amplitude of the response was significantly increased in the HFD group (**Figs. 2B, C, and E** RD 2.62 ± 0.29; HFD 3.18 ± 0.34, $P = 0.01$). Furthermore, we determined that the kinetics of individual $[Ca^{2+}]_i$ transients observed during our in vivo calcium imaging studies were not altered in HFD as compared with RD mice. Hence, changes in the frequency of these signals in these 2 populations are likely to reflect changes in excitability and associated voltage dependent calcium influx, rather than changes in neuronal calcium buffering mechanisms.

Overall, this in vivo calcium study demonstrated that HFD $Na_v1.8$ DRG neurons responded to a nonnoxious mechanical stimulus with $[Ca^{2+}]_i$ transients of significantly higher amplitude compared with RD. This is a critical result as we know that sustained increased $[Ca^{2+}]_i$ is a key component in the signaling pathways leading to axonal degeneration in the peripheral nervous systems.[60,82,109] Therefore, we next investigated the potential causal connections between this increased $[Ca^{2+}]_i$ in vivo and axonal degeneration and mechanical allodynia in this model.

3.3. Morphological changes in mitochondria preceded mechanical allodynia and small-fiber degeneration in diabetic mice

High $[Ca^{2+}]_i$ can contribute to axonal damage by altering mitochondrial morphology and function.[12] To determine if the increased $[Ca^{2+}]_i$ we observed in HFD DRG neurons in vivo calcium imaging affects mitochondria in this way, we used EM to analyze mitochondrial morphology in the somas and in the axons of RD and HFD DRG neurons (**Figs. 3 and 4**). Although mitochondria have been implicated in the pathology of PDN,[110,111] we know little about the extent or timing of mitochondrial alterations as it relates to pathogenesis. We previously showed that the typical hallmarks of PDN, neuropathic pain behavior, and small-fiber neuropathy occur in mice on a HFD in the form of mechanical allodynia (6 weeks after starting the diet) and decreased nerve fiber density (8 weeks after starting the diet).[51] To evaluate whether mitochondria in DRG neurons show plasticity in HFD mice even before the onset of PDN, we analyzed mitochondrial morphology in the somas of small-diameter neurons in DRG, that are primarily nociceptors, taken from mice fed either RD or HFD for 2 or 10 weeks (**Fig 3**; Suppl Fig. 2a, available at http://links.lww.com/PAIN/B424). Using a EM analysis protocol previously described,[83,116] we observed that parameters such as aspect ratio, roundness, and form factor were unaffected by diet (Suppl Fig. 2C-E, available at http://links.lww.com/PAIN/B424). Whereas area, perimeter, and interconnectivity (lower score indicates fragmentation) were significantly decreased in DRG neurons in HFD mice compared with RD mice at 10 weeks after starting the diet (**Fig. 3**) (area: RD 0.13 ± 0.02 vs HFD 0.08 ± 0.01; $P = 0.001$, perimeter: RD 1.54 ± 0.10 vs HFD 1.13 ± 0.07; $P = 0.03$, and interconnectivity: RD 0.09 ± 0.00 vs HFD 0.07± 0.00; $P < 0.0001$). Interestingly, mitochondria of HFD DRG neurons displayed fragmented morphology as early as 2 weeks after diet commencement, preceding the onset of mechanical allodynia and small-fiber degeneration (**Fig. 3**) (area: RD 0.17 ± 0.02 vs HFD 0.08 ± 0.01; $P < 0.0001$, perimeter: RD 1.54 ± 0.08 vs HFD 1.11 ± 0.06; $P < 0.0001$, and interconnectivity: RD 0.11 ± 0.00 vs HFD 0.08 ± 0.00; $P < 0.0001$). In addition, in mice fed a HFD for 10 weeks, we observed fragmented mitochondria in the axons of DRG neurons extending to the epidermal–dermal junction (**Fig. 4**) (area: RD 0.08 ± 0.01 vs HFD 0.05 ± 0.01; $P = 0.01$, perimeter: RD 1.05 ± 0.07 vs HFD 0.86 ± 0.05; $P = 0.02$, and interconnectivity: RD 0.07 ± 0.00 vs HFD 0.06 ± 0.00; $P = 0.01$). The observed altered mitochondria morphology with fragmented mitochondria in the long peripheral axons of the DRG nerve endings in the skin could be particularly relevant from the point of view of axonal degeneration.

3.4. Deleting the mitochondrial calcium uniporter from $Na_v1.8$-expressing dorsal root ganglion neurons prevented mechanical allodynia and small-fiber degeneration in diabetic mice

Our laboratory has shown that reducing $Na_v1.8$-expressing DRG neuron hyperexcitability not only reversed mechanical allodynia in the HFD mouse model of PDN but also reversed small-fiber degeneration.[51] In this model, hyperexcitability in $Na_v1.8$-expressing DRG neurons was accompanied by increased $[Ca^{2+}]_i$.[51] As mentioned above, increased $[Ca^{2+}]_i$ can contribute to axonal damage by altering mitochondrial morphology and function.[12] The intramitochondrial $[Ca^{2+}]_i$ may be critical in the regulation of mitochondrial dynamics and morphology.[19,35,48] A major pathway for mitochondrial calcium influx is through the MCU.[9,37]

To test whether calcium entry into DRG neuron mitochondria has a role in the pathogenesis of PDN, we deleted MCU from $Na_v1.8$-expressing DRG neurons by crossing $Na_v1.8$-Cre; Ai9 mice with MCU-floxed mice ($MCU^{flox/flox}$) kind gift from Jeffery Molkentin.[54] To demonstrate that this manipulation did not cause DRG developmental defects,[10] we performed in situ hybridization of $Na_v1.8$, NF200, and CGRP to characterize the DRG neuronal populations. The number of DRG neurons labeled with $Na_v1.8$ (**Fig. 5** RD-Het 67.10 ± 4.85 vs RD-Homo 65.79 ± 9.19; $P = 0.99$, HFD-Het 62.74 ± 5.03 vs HFD-homo 65.45 ± 9.95; $P = 0.94$) was no different in the $Na_v1.8$-Cre; Ai9; $MCU^{flox/+}$ heterozygous (Het) and $Na_v1.8$-Cre; Ai9; $MCU^{flox/flox}$ homozygous (Homo) mice. Moreover, we found no significant difference in the number of DRG neurons that were positive for CGRP (**Fig. 5** RD-Het 51.79 ± 5.73 vs RD-Homo 63.38 ± 18.41; $P = 0.71$, HFD-Het 54.31 ± 5.20 vs HFD-homo 63.98 ± 7.35; $P = 0.80$), a marker that mostly identifies the peptidergic neurons as well as

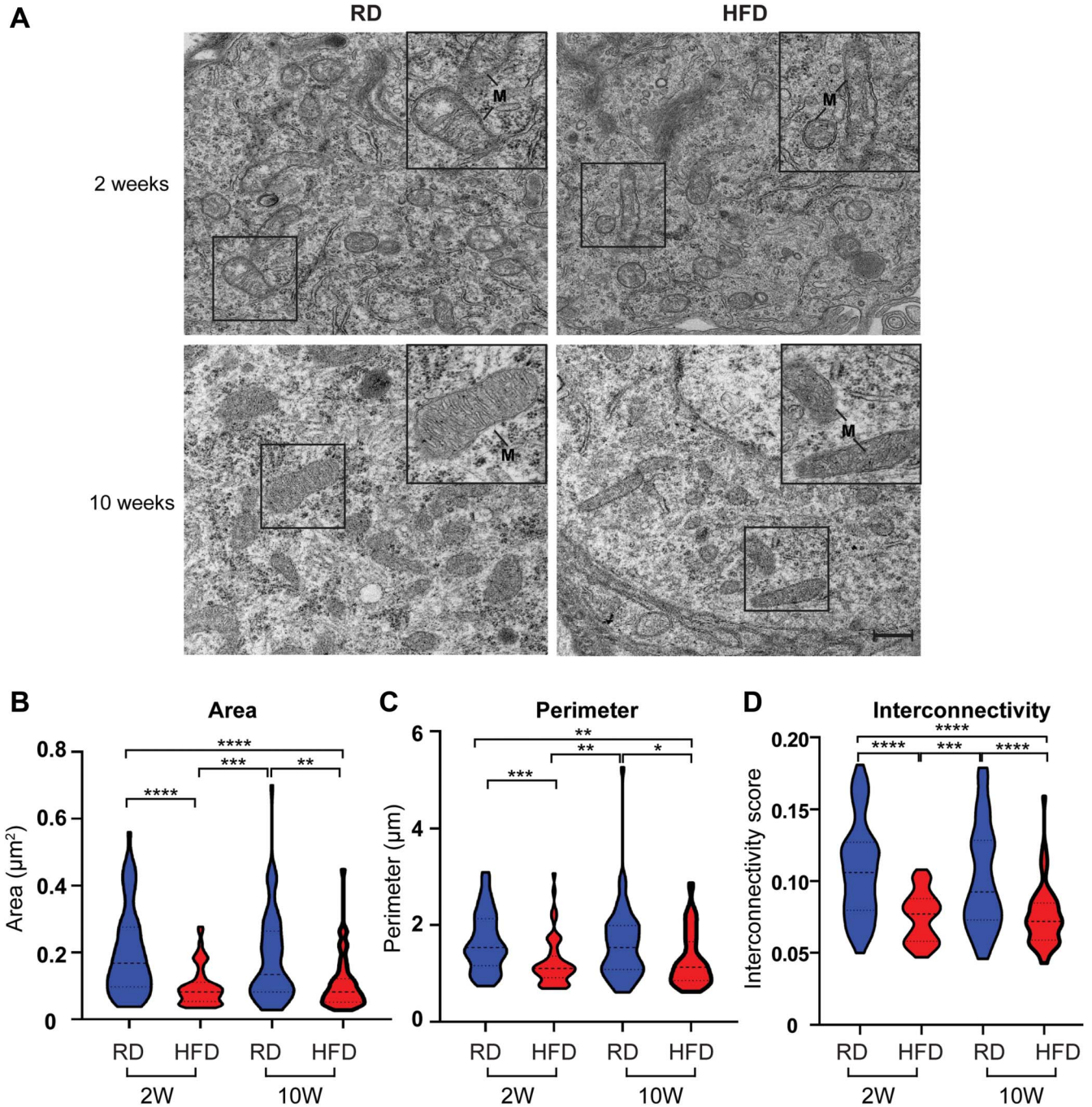

Figure 3. Morphological measurements of mitochondria in small diameter DRG neuronal cell bodies demonstrate fragmented mitochondria in mice fed a HFD. (A) Electron micrographs of small diameter DRG neurons from animals fed a RD (left) or HFD (right) after 2 (top) and 10 (bottom) weeks on diet. (B–D) Comparison of area, perimeter, and interconnectivity of mitochondria between mice fed a RD or HFD at 2 and 10 weeks (W). $^{**}P < 0.01$ and $^{****}P < 0.0001$. Scale bar represents 500 nm. M indicates mitochondria. DRG, dorsal root ganglion; HFD, high-fat diet; RD, regular diet.

with IB4 staining which identifies the nonpeptidergic nociceptive neurons[8,101] (**Fig. 5** RD-Het 27.88 ± 3.78 vs RD-Homo 29.10 ± 5.08; $P = 0.99$, HFD-Het 29.88 ± 1.59 vs HFD-homo 28.02 ± 2.11; $P = 0.96$). This result indicates that these mice have normal segregation of peptidergic and nonpeptidergic nociceptors after neurogenesis.[11,97] In addition, no changes were seen in the large diameter mechanoreceptors that express neurofilament-200 (NF200) as well (**Fig. 5** 5 RD-Het 26.68 ± 4.23 vs RD-Homo 20.25 ± 3.41, $P = 0.42$, HFD-Het 29.39 ± 5.55 vs HFD-homo 27.66 ± 3.61; $P = 0.96$). Furthermore, as in wild type mice fed a HFD, both Het and Homo mice fed HFD developed obesity (Suppl Fig. 3a, available at http://links.lww.com/PAIN/B424, RD-Het 26.41 ± 3.19; RD-Homo 27.37 ± 1.86; HFD-Het 38.27 ± 5.69; and HFD-Homo 40.16 ± 6.87) and glucose intolerance (Suppl Fig. 3b, c, available at http://links.lww.com/PAIN/B424, GTT at 120 minutes: RD-Het 137.60 ± 5.96; RD-Homo 129.70 ± 8.43; HFD-Het 416.40 ± 31.87; and HFD-Homo 358.10 ± 37.41), demonstrating that the MCU deletion did not alter the metabolic profile of mice in this model.

We then tested both Het and Homo mice for mechanical allodynia using von Frey withdrawal threshold measurements, as

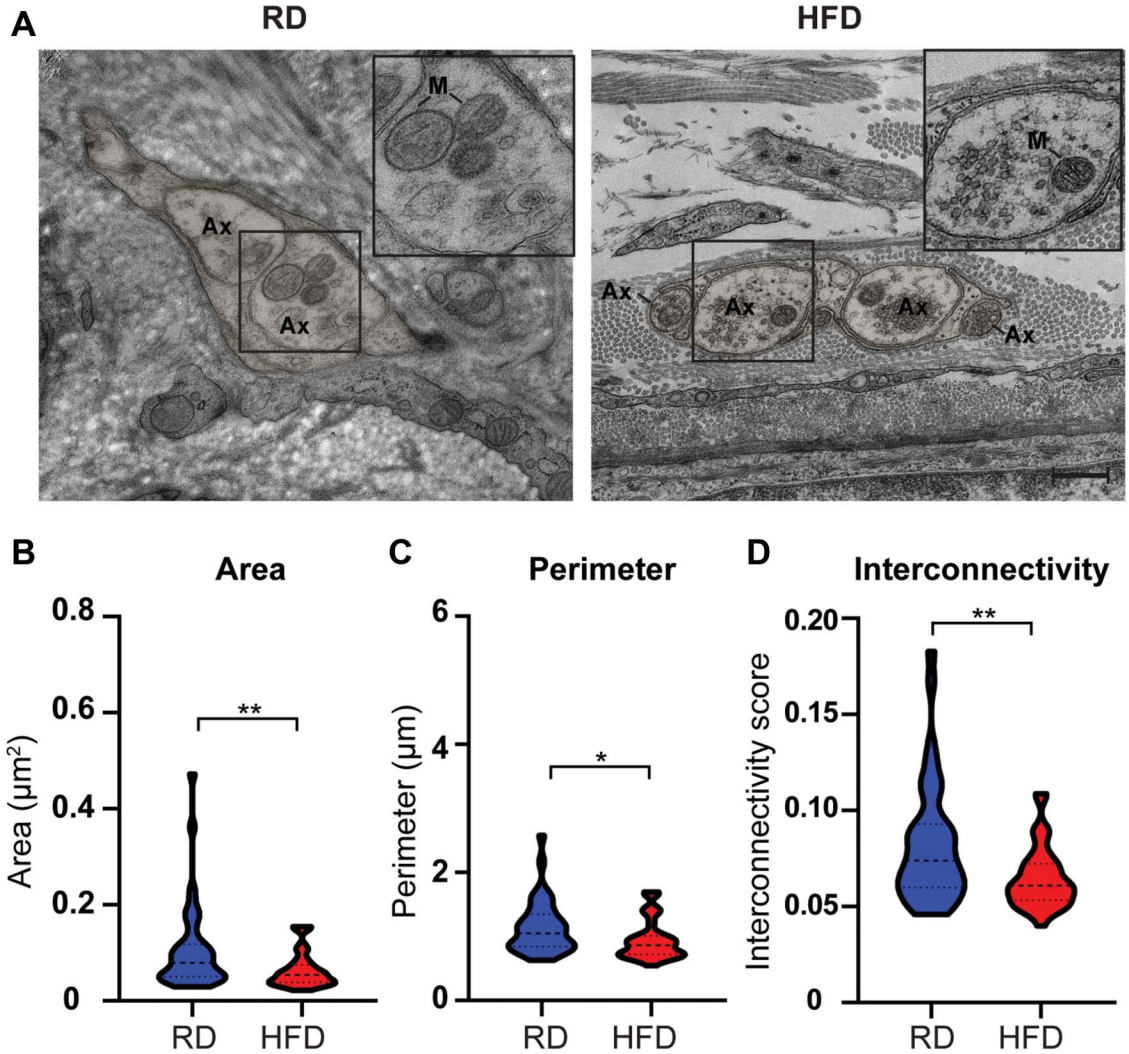

Figure 4. Morphological measurements of mitochondria in axons within Remak bundles in hind paw skin demonstrate fragmented mitochondria in mice fed a HFD. (A) Electron micrographs of Remak bundles from animals fed a RD (left) or HFD (right) at 10 weeks on diet. (B–D) Comparison of area, perimeter, and interconnectivity of mitochondria between mice fed a RD or HFD at 10 weeks. *$P < 0.05$ and **$P < 0.01$. Scale bar represents 500 nm. Ax, M indicates axons and mitochondria, respectively. HFD, high-fat diet; RD, regular diet.

described.[13,51,71] We have previously shown that mice fed an HFD developed mechanical allodynia 6 weeks after diet commencement. In Het mice fed the HFD for 10 weeks, the withdrawal threshold was significantly reduced compared with RD-Het mice (RD-Het 1.03 ± 0.26 vs HFD-Het 0.30 ± 0.18; $P = 0.0013$), indicating mechanical allodynia in this group (**Fig. 6A**). By contrast, HFD-Homo mice had normal withdrawal thresholds (0.91 ± 0.47; $P = 0.0018$) compared with the HFD-Het, indicating that deleting the MCU from $Na_v1.8$-expressing DRG neurons prevented the establishment of mechanical allodynia in this model of PDN. We did not observe mechanical allodynia in RD-Homo (1.17 ± 0.63 vs RD-Het $P = 0.92$), indicating that MCU deletion did not alter mechanical sensation in otherwise metabolically normal mice. To further characterize the pain phenotype, we tested for thermal sensitivity using the Hargreaves test[27] in both Het and Homo mice fed either an RD or HFD for 10 weeks. We observed that there were no thermal sensitivity deficits between these 4 groups (**Fig. 6B**; RD-Het 5.63 ± 0.60 vs HFD-Het 5.60 ± 0.47 $P > 0.99$; RD-Homo 5.19± 1.40 vs HFD-Homo 6.08 ± 1.58 $P = 0.57$).

We next tested whether inhibiting MCU-mediated calcium uptake in $Na_v1.8$-expressing DRG neurons protected against small-fiber degeneration. Using confocal microscopy, we examined skin innervation in both $Na_v1.8$-Cre; Ai9; $MCU^{flox/+}$ heterozygous (Het) and $Na_v1.8$-Cre; Ai9; $MCU^{flox/flox}$ homozygous (Homo) mice in which $Na_v1.8$-positive afferents in the skin were labeled red with td-Tomato reporter protein. Het and Homo mice were fed a RD or HFD for 10 weeks (**Fig. 7**). We saw normal innervation in animals fed a RD regardless of genotype (RD-Het 0.03 ± 0.00; RD-Homo 0.04 ± 0.01); thus, deleting MCU from $Na_v1.8$-expressing DRG neurons did not interfere with normal neurite outgrowth. We observed a significant reduction in IENF density in HFD-Het mice (0.02 ± 0.00) compared with RD-Het ($P = 0.0055$) and RD-Homo ($P = 0.0014$). Using an antibody against the protein gene product 9.5 (PGP 9.5), a pan-neuronal marker used for calculating IENF density and for diagnosing small-fiber neuropathies,[58,98] we have previously excluded the possibility that the results reflected abnormal td-Tomato expression or transport in HFD mice.[51] In HFD-Homo mice (0.04 ± 0.01), we saw significantly improved skin innervation compared with the HFD-Het mice ($P = 0.0005$), demonstrating that deleting MCU from $Na_v1.8$-expressing DRG neurons prevented axonal degeneration in the HFD mouse model of PDN.

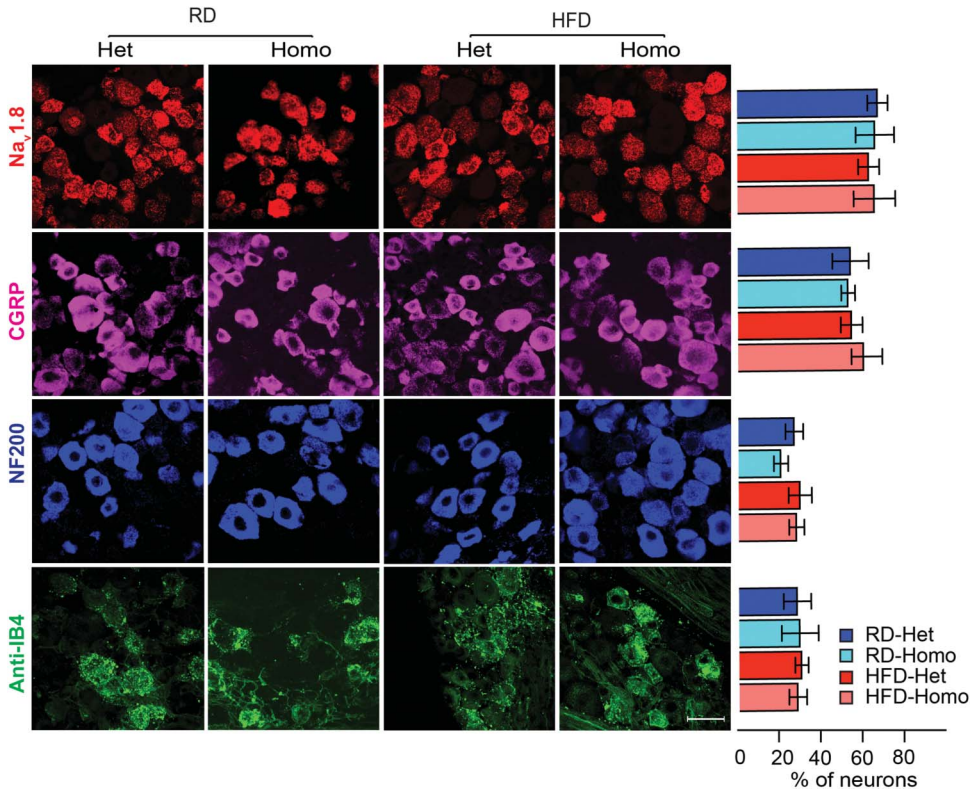

Figure 5. Deletion of the MCU from the Nav1.8-expressing DRG neurons does not alter the DRG neuronal subpopulations. Confocal images and quantification of in situ hybridization of Nav1.8 (red), CGRP (magenta), NF200 (blue), and immunohistochemistry of IB4 (green) from MCU heterozygous (Het) and homozygous (Homo) mice fed a RD or HFD. Scale bar represents 50 μm. DRG, dorsal root ganglion; HFD, high-fat diet; MCU, mitochondrial calcium uniporter; RD, regular diet.

3.5. Deleting the mitochondrial calcium uniporter from Na$_v$1.8-expressing dorsal root ganglion neurons restored normal mitochondrial morphology in diabetic mice

We observed fragmented mitochondrial morphology in DRG neurons in the HFD mouse model of PDN (**Fig. 3**). To investigate if deleting the MCU would reverse axonal degeneration and mechanical allodynia by restoring normal mitochondrial morphology and dynamics in Na$_v$1.8-expressing DRG neurons, we used EM to analyze the somas of small-diameter neurons in DRG, that are primarily nociceptors, taken from Na$_v$1.8-Cre; Ai9; MCU$^{flox/flox}$ homozygous (Homo) and heterozygous (Het) mice fed either a RD or HFD for 10 weeks (**Fig. 8**). We observed a statistically significant reduction in the area (RD-Het 0.15 ± 0.01; HFD-Het 0.08 ± 0.01; $P < 0.0001$), perimeter (RD-Het 1.44 ± 0.01; HFD-Het 1.14 ± 0.01; $P < 0.0001$), and interconnectivity (RD-Het 0.10 ± 0.00; HFD-Het 0.07 ± 0.00; $P < 0.0001$) of mitochondria in DRG neurons of HFD-Het mice compared with RD-Het mice, thus revealing fragmented mitochondria morphology as part of

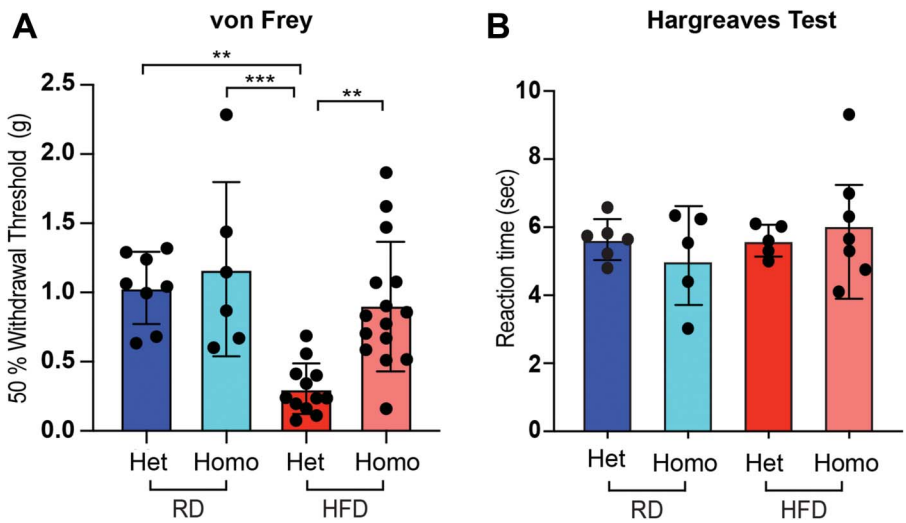

Figure 6. Deletion of the MCU from Na$_v$1.8-expressing DRG neurons prevented mechanical allodynia among neurons in the HFD model at 10 weeks on diet. (A) Mechanical allodynia measured using the von Frey. (B) Thermal sensitivity measured using the Hargreaves test. $^{**}P < 0.01$, $^{***}P < 0.001$. DRG, dorsal root ganglion; HFD, high-fat diet; MCU, mitochondrial calcium uniporter.

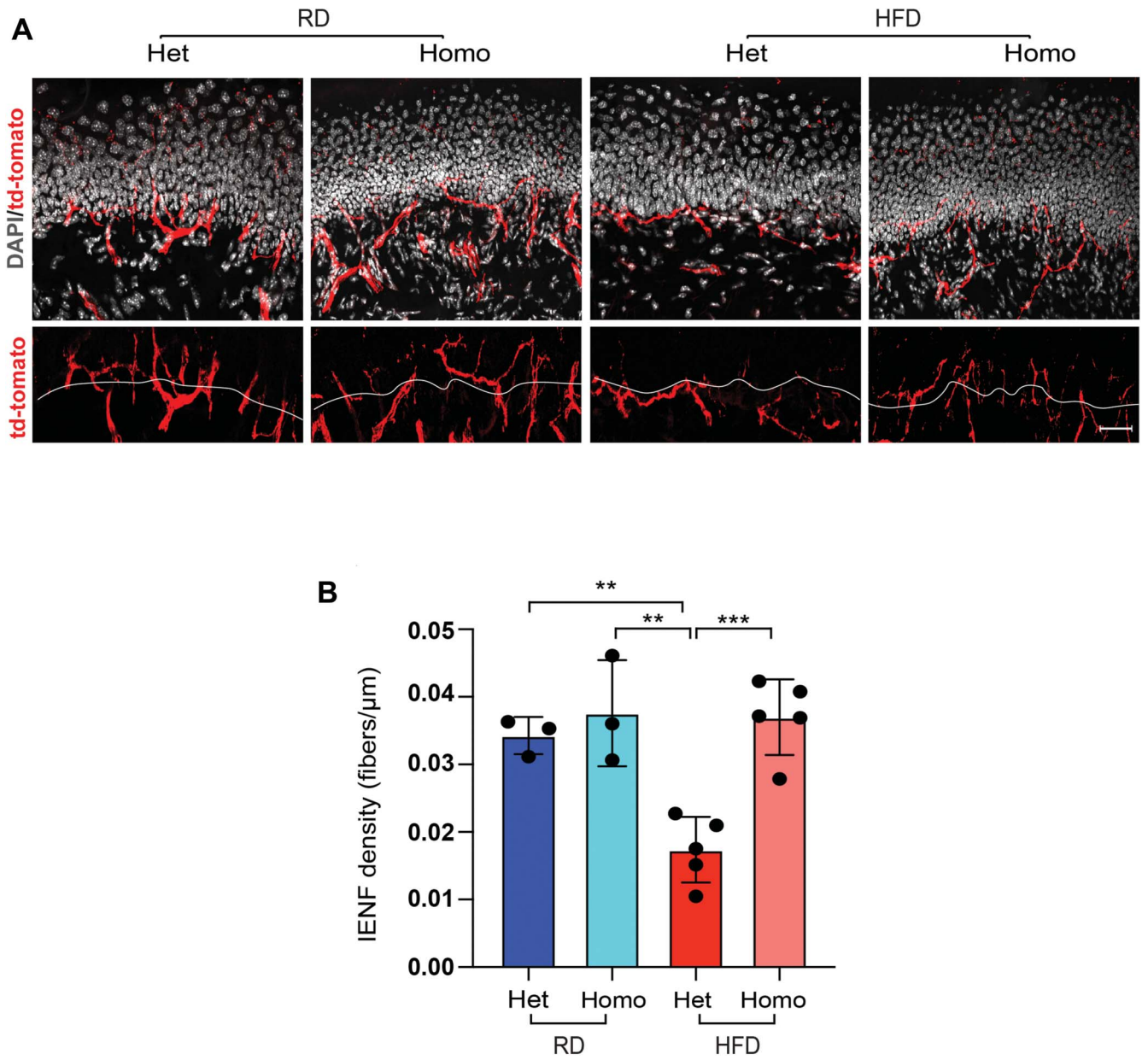

Figure 7. Deletion of the MCU from $Na_v1.8$-expressing DRG neurons prevented small fiber degeneration in the HFD model. (A) Confocal analysis of $Na_v1.8$-expressing fibers (labeled with td-tomato) from the skin of RD and HFD mice with heterozygous or homozygous deletions of MCU showing td-tomato (red) and merged images with the nuclear marker DAPI (gray). White solid line demarcates the epidermal–dermal junction. Scale bars represent 50 μm. (B) Quantification of the intraepidermal nerve fiber density. $^{**}P < 0.01$ and $^{***}P < 0.001$. DRG, dorsal root ganglion; HFD, high-fat diet; MCU, mitochondrial calcium uniporter; RD, regular diet.

the phenotype of this PDN model. No difference in morphology was noted between RD-Het and RD-Homo mice (area: 0.13 ± 0.01; $P = 0.82$; perimeter: 1.36 ± 0.05; $P > 0.99$; and interconnectivity: 0.09 ± 0.00; $P = 0.55$), indicating that deleting the MCU does not itself alter mitochondria morphology. However, Homo mice maintained normal mitochondrial morphology even while on the HFD (area, 0.12 ± 0.01; perimeter, 1.34 ± 0.04; and interconnectivity, 0.09 ± 0.00) (**Fig. 8**), demonstrating that the selective deletion within $Na_v1.8$-expressing DRG neurons was protective against mitochondrial fragmentation in these mice.

4. Discussion

Using the HFD mouse model of PDN, we found that mitochondrial proteins were DE in DRG neurons. Specifically, we found that mitochondrial proteins involved in fission were elevated in this model and that the mitochondria in DRG nociceptors of these mice displayed a fragmented morphology before the onset of mechanical allodynia and small-fiber degeneration. Blocking MCU-mediated calcium entry into the mitochondria of $Na_v1.8$-expressing DRG neurons restored normal mitochondrial morphology and prevented small-fiber degeneration and mechanical allodynia. These studies suggest a molecular cascade linking neuropathic pain to axonal degeneration in PDN. In particular, nociceptor hyperexcitability and the associated increase in intracellular calcium concentration could lead to excessive calcium entry into mitochondria mediated by the MCU complex. This would in turn result in increased calcium-dependent mitochondrial fission and ultimately contribute to small-fiber degeneration and neuropathic pain in PDN (**Fig. 9**).

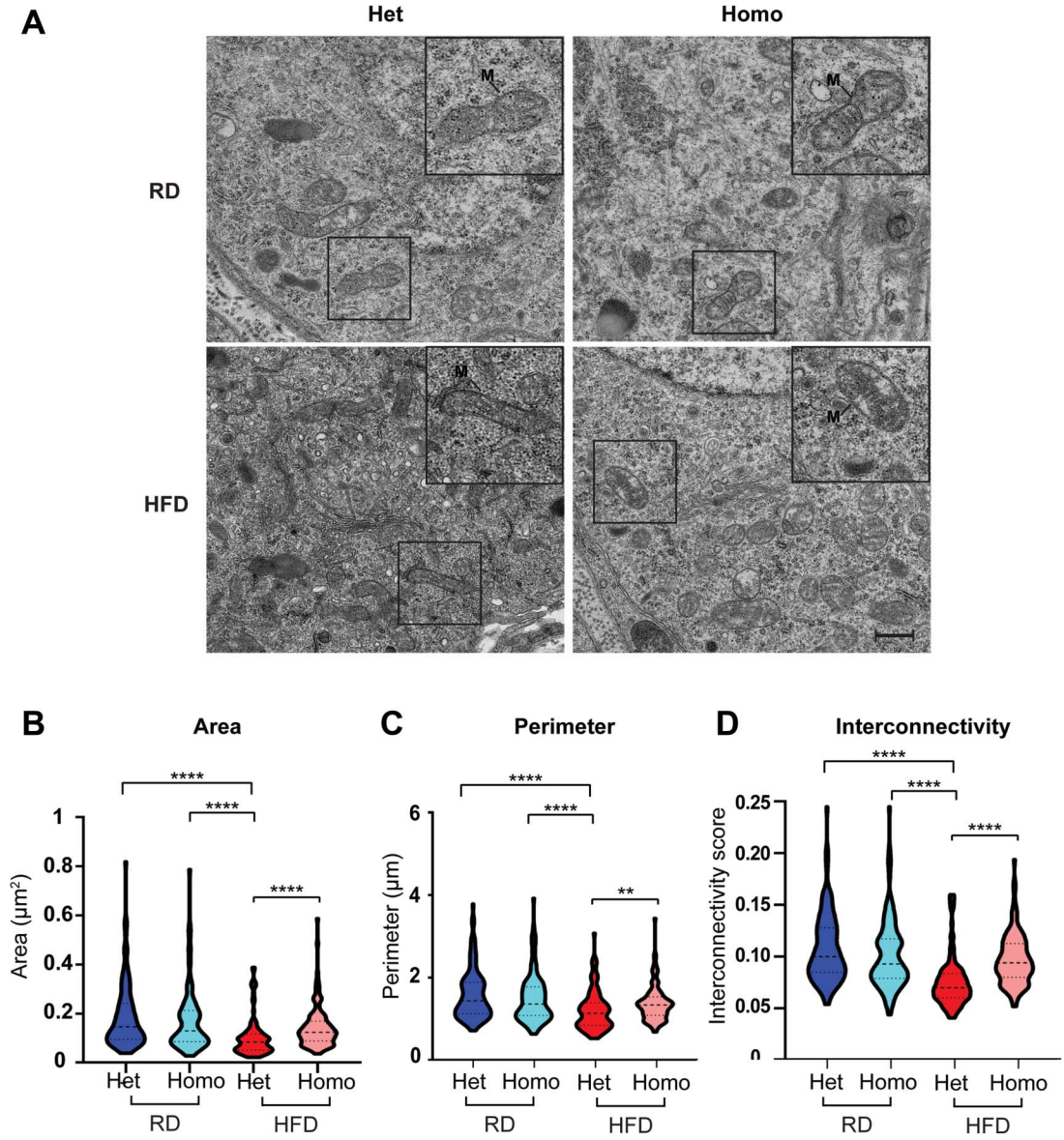

Figure 8. Morphological measurements of mitochondria in animals with heterozygous or homozygous deletion of MCU fed either a RD or HFD. (A) Electron micrographs from small diameter DRG neurons from RD (top) and HFD (bottom) mice with heterozygous (left) or homozygous (right) deletions of MCU. Images were taken after 10 weeks on diet. (B–D) Comparison of area, perimeter, and interconnectivity of mitochondria between mice fed a RD or HFD at 10 weeks. $^{**}P < 0.01$ and $^{****}P < 0.0001$. Scale bar represents 500 nm, and M indicates mitochondria. DRG, dorsal root ganglion; HFD, high-fat diet; MCU, mitochondrial calcium uniporter; RD, regular diet.

Our findings indicate that deleting the MCU from $Na_v1.8$-expressing DRG neurons prevented PDN by restoring normal mitochondria morphology and dynamics[21] in DRG neurons of diabetic mice. Defects in mitochondrial morphology and dynamics can compromise mitochondrial functions and so affect neuronal survival and function.[22,34,69] DRG neurons are especially dependent on efficient mitochondrial dynamics because of their unique morphology and long axons.[20,63,66,91] Our results raise questions about the specific mechanism through which deleting MCU from $Na_v1.8$-expressing DRG neurons restores normal mitochondria morphology. Fragmented mitochondrial morphology is associated with excessive fission,[21,92] and there is cross-talk between the MCU and mitochondrial fission under conditions associated with intracellular calcium overload.[47] In other models of calcium overload, such as myocardial I/R injury, MCU is upregulated[47,120] and mitochondrial fission is enhanced.[120] In I/R injury, pharmacologically blocking MCU reduced myocardial infarction by alleviating mitochondria fission.[120]

We demonstrated that HFD-induced PDN increased calcium both ex vivo[51] and in vivo in $Na_v1.8$-expressing DRG neurons in response to mechanical stimulation (**Fig. 3**). These data indicate that calcium influx through the MCU could underlie axonal degeneration in PDN. One possible mechanism is that mitochondria calcium concentration per se acts as an intrinsic signal that regulates mitochondrial morphology. Indeed, calcium influx into mitochondria might affect mitochondrial morphology and dynamics by regulating Drp1 phosphorylation[19,35,48] and, interestingly, inhibiting calcium-dependent mitochondrial fission alleviates capsaicin-induced axonal degeneration.[25] Thus, MCU-mediated calcium influx into the mitochondria could lead to excessive mitochondrial fission and fragmentation in DRG nociceptors in the HFD mouse model of PDN.

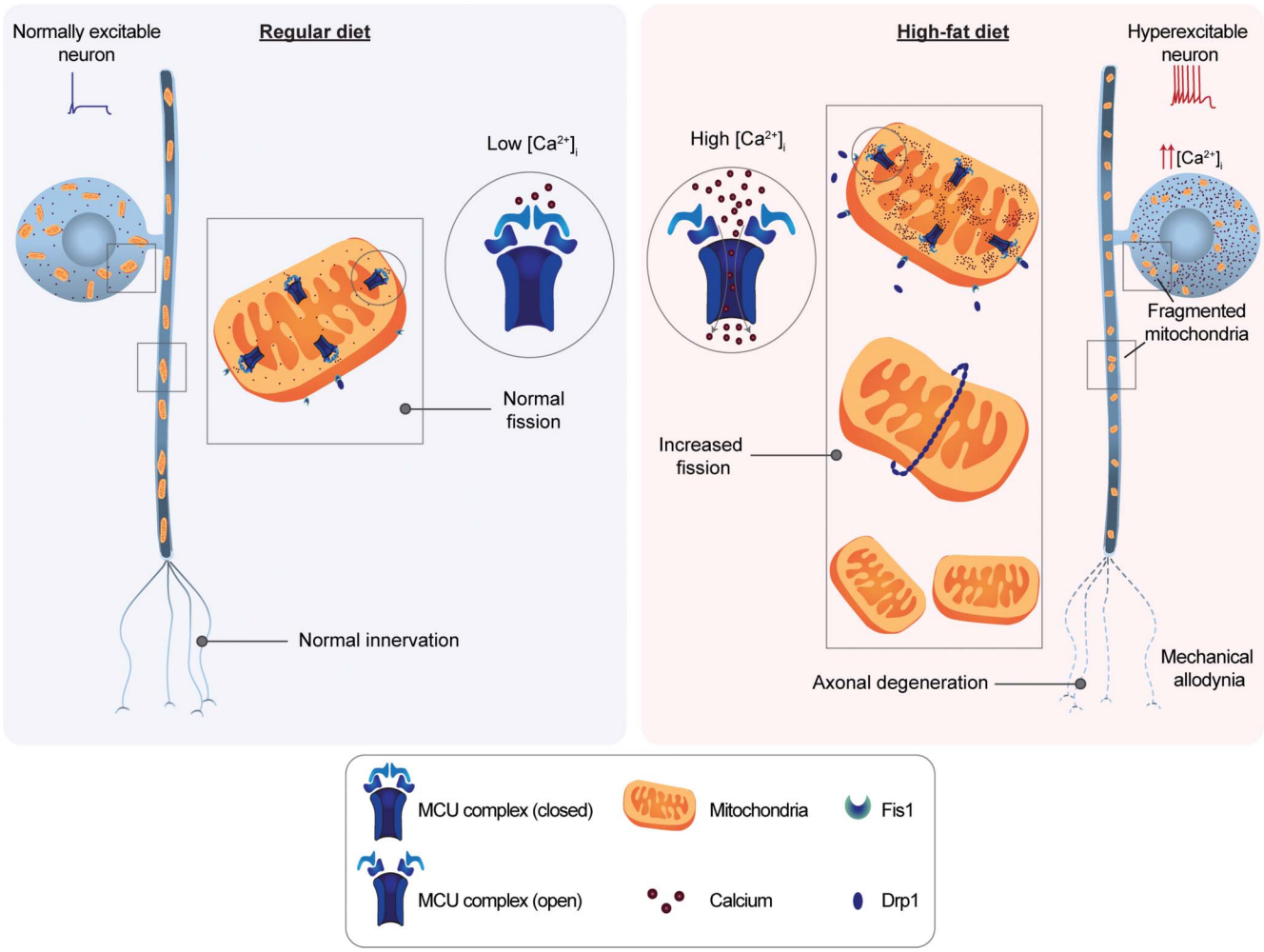

Figure 9. Schematic representation showing hyperexcitability of neurons and increased intracellular calcium in HFD causing the opening of MCU channels leading to increased calcium-dependent mitochondrial fission and ultimately contributing to small-fiber degeneration and neuropathic pain in PDN. PDN, painful diabetic neuropathy; HFD, high-fat diet; MCU, mitochondrial calcium uniporter.

Mitochondrial morphology and dynamics are determined by the balance between fission, fusion, and autophagy,[21,92] suggesting potential mechanisms by which selective deletion of MCU might reverse pathologically fragmented mitochondrial morphology in diabetic DRG neurons. In cystic fibrosis, for instance, deleting MCU blocks autophagy and alleviates the inflammatory response in bronchial cells exposed to pathogen.[88] Inflammation is also implicated in the pathogenesis of PDN.[53,85,106] Autophagy is a constitutively active process in adult DRG neurons and contributes to neuronal survival and neurite growth and regeneration in vitro.[31] Pharmacologically inhibiting autophagic activity, or inducing defective autophagy in transgenic mice, exacerbates the allodynia response and persistence of neuropathic pain.[32] Therefore, it is unlikely that selectively deleting MCU from $Na_V1.8$-expressing DRG neurons prevents neuropathic pain and axonal degeneration by inhibiting autophagic activity. Indeed, we observed that it was possible to resolve mechanical allodynia by restoring mitochondrial morphology and balance between fission and fusion in DRG nociceptors in the HFD mouse model of PDN.

Our understanding of the structure and function of the MCU complex has rapidly increased because the pore-forming molecule[9,37] and its regulatory subunits were identified. These include the essential MCU regulator,[93] MCUR1,[67] MCUb,[86] mitochondrial calcium uptake (MICU) 1, MICU2, and MICU3.[81] Using multiplexed quantitative proteomic analyses, we found that DRG neurons in HFD mice had an elevated level of MCUR1, a positive regulator for MICU. This in turn might accelerate the entry of calcium into the mitochondria. Deleting MCU could therefore block excessive calcium entry into nociceptor mitochondria by impairing the function of specific MCU complex components, including MCUR1. In future studies, we plan to test if manipulating individual MCU complex components in this model of PDN, pharmacologically or genetically, influences mitochondrial dynamics and the development of mechanical allodynia and axonal degeneration. Indeed, all components of the MCU complex are pharmacological targets of considerable interest.[4,38,55,88,117]

Balanced uptake of calcium into mitochondria is a key regulator of diverse cellular homeostatic processes, from bioenergetics to cell death.[46,68] The data presented here demonstrate for the first time that MCU, the major responsible for calcium uptake, has been selectively deleted in DRG sensory neurons. Previous studies of MCU knockout mice showed phenotypic variability, including a viable strain with a modest phenotype in a mixed genetic background,[79] lethal or semiviable phenotype in an inbred background,[75] and a tissue-specific conditional knockout with an important role in cardiac homeostasis.[65] One explanation for this variability is that perturbing MCU can be influenced by additional factors, such as genetic background and cell-specific vulnerability. In light of these

previous results, it was important for us to demonstrate that selectively deleting MCU from DRG neurons did not alter normal development and function in mice fed a RD (**Figs. 5** and **6a, b**). These results are corroborated by reports of viable and fertile fly MCU mutants with no gross morphological or behavioral defects,[28,105] as well as studies in mice and worms in which deletion of MCU orthologs is benign at the organismal level under "basal" conditions.[79,118] These findings have been interpreted as evidence that the MCU is a major pathway for calcium influx into the mitochondria when the intracellular concentration of calcium rises above the mitochondrial set-point.[9,37] The MCU has a relatively low affinity for calcium, so the cytosolic calcium concentration needs to be approximately 600 nM for significant transport of calcium into the mitochondria to occur.[52] This feature makes the MCU channel a particularly appealing therapeutic target for a variety of pathological conditions associated with increased intracellular calcium.[9,37] MCU blockers will selectively block the excessive calcium entry into the mitochondria only in cell types with calcium overload but will have minimal off-target effects on other cells with calcium concentration below the mitochondrial set-point.

Painful symptoms vary among patients with PDN,[7] leading to different sensory phenotypes[7,103] with different molecular mechanisms.[113] Such distinctions have been targeted with a view to improving clinical trial outcomes and therapeutic efficacy.[5,6,104,107,112] In patients with PDN, mechanical allodynia is commonly observed together with thermal hypoesthesia, particularly at later stages of the disease.[7,17,84,103] Similarly, in the HFD model, as in other mouse models of PDN,[15,102] mice ultimately develop thermal hypoalgesia but not until 16 weeks after starting HFD.[76] After 10 weeks on HFD, mice display mechanical allodynia without thermal hypoalgesia[71,72,76](**Fig. 6B**). Given that sensory phenotypes are heterogeneous and vary with disease stage,[7] therapeutics targeting MCU could be most beneficial in the subgroup of patients with PDN in the early stages of the disease displaying mainly mechanical allodynia. Mechanical allodynia is common in patients with PDN,[71,72] although the relative contribution of its static and dynamic components, which are important in the clinic, may not be precisely duplicated in mouse models.[103,113]

In summary, our studies introduce a novel pathway linking MCU-mediated increased calcium influx into the mitochondria of $Na_v1.8$-expressing DRG neurons and mitochondrial dynamics to axonal degeneration and mechanical allodynia in PDN. From a translational perspective, we propose that selectively targeting calcium entry into nociceptor mitochondria may be a novel, effective, and disease-modifying approach to therapeutic interventions that not only treat neuropathic pain more effectively but also reverse the pathological trigger of neuropathic pain and restore nerve terminal axonal health. This could ultimately mean more long-lasting relief for patients suffering from PDN and a transformation in the way small-fiber degeneration is treated, replacing the largely ineffective approaches that are currently available. Specifically, we predict that drugs that block calcium influx into DRG nociceptor mitochondria, such as those capable of modulating the MCU complex,[4,38,55,88,117] will effectively treat PDN. Moreover, the relationships we reveal among MCU-mediated increases in calcium influx into mitochondria, mitochondria dynamics, mitochondria morphology, and axonal degeneration are likely to inform studies of other neurodegenerative diseases involving similar underlying events, such as amyotrophic lateral sclerosis[114] or Parkinson disease.[62]

Conflict of interest statement

The authors have no conflicts of interest to declare.

Acknowledgements

This work was supported by NIH R01 and NIH HEAL initiative supplement R01 NS104295-01, NIH/NIAMS R01 AR077691-01 (D.M.M.) and NIH and NIH/Rush University Medical Center 1R01AR064251-01 (R.J.M., A.M.M.). Jeffery Savas laboratory is supported in part by AG061787. The authors thank Dr. Rajeshwar Awatramani for helpful discussions. The authors thank Dr. Shingo Ishihara for the technical assistance with the paw hyperalgesia experiments and Dr. Vania Apkarian's lab and Maria Virginia Centeno for allowing us to use the Ugo Basile apparatus. The authors thank Lennell Reynolds Jr at the Northwestern University Center for Advanced Microscopy for help with the electron microscope. The authors thank Dr. Jeffery Molkentin (Cincinnati Children's Hospital Medical Center) for the generous gift of the $MCU^{fl/fl}$ mice.

Author contributions: D.S. George performed proteomic analysis, in vivo calcium analysis, EM analysis, in situ hybridization, confocal imaging, statistical analysis, figures, and article revision. S. Hackelberg performed Fura-2 calcium imaging, statistical analysis, and article revision. N.D. Jayaraj performed von Frey behavioral studies, immunohistochemical labeling, confocal imaging, and statistical analysis, mouse breeding, administration of HFD, testing for diabetes, evaluation by immunofluorescence of intraepidermal nerve fiber (IENF) density, figures, and article revision. D. Ren performed mouse breeding, administration of HFD, testing for diabetes, DRG cell culture, and in vivo calcium surgery and experimentation. S.L. Edassery and J.N. Savas performed TMT 16pLex analysis. R.E. Miller setup and performed in vivo calcium imaging. A.-M. Malfait aided in the analysis of the in vivo calcium imaging. C. Rathwell aided in IENF quantification. D.M. Menichella supervised the project. D.M. Menichella and D.S. George drafted the article. D.M. Menichella and R.J. Miller edited the article. All authors read and approved the article.

Appendix A. Supplemental digital content

Supplemental digital content associated with this article can be found online at http://links.lww.com/PAIN/B424. http://links.lww.com/PAIN/B425 and http://links.lww.com/PAIN/B426.

Article history:
Received 23 January 2021
Received in revised form 25 May 2021
Accepted 18 June 2021
Available online 2 July 2021

References

[1] Abbott CA, Malik RA, van Ross ER, Kulkarni J, Boulton AJ. Prevalence and characteristics of painful diabetic neuropathy in a large community-based diabetic population in the U.K. Diabetes care 2011;34:2220–4.
[2] American Diabetes A. Diagnosis and classification of diabetes mellitus. Diabetes Care 2011;34(suppl 1):S62–69.
[3] Andersson DA, Gentry C, Light E, Vastani N, Vallortigara J, Bierhaus A, Fleming T, Bevan S. Methylglyoxal evokes pain by stimulating TRPA1. PLoS One 2013;8:e77986.
[4] Arduino DM, Wettmarshausen J, Vais H, Navas-Navarro P, Cheng Y, Leimpek A, Ma Z, Delrio-Lorenzo A, Giordano A, Garcia-Perez C, Medard G, Kuster B, Garcia-Sancho J, Mokranjac D, Foskett JK, Alonso MT, Perocchi F. Systematic identification of MCU modulators by orthogonal interspecies chemical screening. Mol Cell 2017;67:711–23.e717.

[5] Attal N, Bouhassira D, Baron R, Dostrovsky J, Dworkin RH, Finnerup N, Gourlay G, Haanpaa M, Raja S, Rice AS, Simpson D, Treede RD. Assessing symptom profiles in neuropathic pain clinical trials: can it improve outcome?. Eur J Pain 2011;15:441–3.
[6] Baron R, Forster M, Binder A. Subgrouping of patients with neuropathic pain according to pain-related sensory abnormalities: a first step to a stratified treatment approach. Lancet Neurol 2012;11:999–1005.
[7] Baron R, Tolle TR, Gockel U, Brosz M, Freynhagen R. A cross-sectional cohort survey in 2100 patients with painful diabetic neuropathy and postherpetic neuralgia: differences in demographic data and sensory symptoms. PAIN 2009;146:34–40.
[8] Basbaum AI, Bautista DM, Scherrer G, Julius D. Cellular and molecular mechanisms of pain. Cell 2009;139:267–84.
[9] Baughman JM, Perocchi F, Girgis HS, Plovanich M, Belcher-Timme CA, Sancak Y, Bao XR, Strittmatter L, Goldberger O, Bogorad RL, Koteliansky V, Mootha VK. Integrative genomics identifies MCU as an essential component of the mitochondrial calcium uniporter. Nature 2011;476:341–5.
[10] Belmadani A, Jung H, Ren D, Miller RJ. The chemokine SDF-1/CXCL12 regulates the migration of melanocyte progenitors in mouse hair follicles. Differentiation 2009;77:395–411.
[11] Bennett DL, Averill S, Clary DO, Priestley JV, McMahon SB. Postnatal changes in the expression of the trkA high-affinity NGF receptor in primary sensory neurons. Eur J Neurosci 1996;8:2204–8.
[12] Bernardi P, Rasola A. Calcium and cell death: the mitochondrial connection. SubCell Biochem 2007;45:481–506.
[13] Bhangoo SK, Ren D, Miller RJ, Chan DM, Ripsch MS, Weiss C, McGinnis C, White FA. CXCR4 chemokine receptor signaling mediates pain hypersensitivity in association with antiretroviral toxic neuropathy. Brain Behav Immun 2007;21:581–91.
[14] Bierhaus A, Fleming T, Stoyanov S, Leffler A, Babes A, Neacsu C, Sauer SK, Eberhardt M, Schnolzer M, Lasitschka F, Neuhuber WL, Kichko TI, Konrade I, Elvert R, Mier W, Pirags V, Lukic IK, Morcos M, Dehmer T, Rabbani N, Thornalley PJ, Edelstein D, Nau C, Forbes J, Humpert PM, Schwaninger M, Ziegler D, Stern DM, Cooper ME, Haberkorn U, Brownlee M, Reeh PW, Nawroth PP. Methylglyoxal modification of Nav1.8 facilitates nociceptive neuron firing and causes hyperalgesia in diabetic neuropathy. Nat Med 2012;18:926–33.
[15] Biessels GJ, Bril V, Calcutt NA, Cameron NE, Cotter MA, Dobrowsky R, Feldman EL, Fernyhough P, Jakobsen J, Malik RA, Mizisin AP, Oates PJ, Obrosova IG, Pop-Busui R, Russell JW, Sima AA, Stevens MJ, Schmidt RE, Tesfaye S, Veves A, Vinik AI, Wright DE, Yagihashi S, Yorek MA, Ziegler D, Zochodne DW. Phenotyping animal models of diabetic neuropathy: a consensus statement of the diabetic neuropathy study group of the EASD (Neurodiab). J Peripher Nerv Syst 2014;19:77–87.
[16] Bult CJ, Blake JA, Smith CL, Kadin JA, Richardson JE; Mouse Genome Database G. Mouse genome database (MGD) 2019. Nucleic Acids Res 2019;47:D801–6.
[17] Callaghan BC, Cheng HT, Stables CL, Smith AL, Feldman EL. Diabetic neuropathy: clinical manifestations and current treatments. Lancet Neurol 2012;11:521–34.
[18] Calvo SE, Clauser KR, Mootha VK. MitoCarta2.0: an updated inventory of mammalian mitochondrial proteins. Nucleic Acids Res 2016;44: D1251–1257.
[19] Cereghetti GM, Stangherlin A, Martins de Brito O, Chang CR, Blackstone C, Bernardi P, Scorrano L. Dephosphorylation by calcineurin regulates translocation of Drp1 to mitochondria. Proc Natl Acad Sci U S A 2008;105:15803–8.
[20] Chada SR, Hollenbeck PJ. Mitochondrial movement and positioning in axons: the role of growth factor signaling. J Exp Biol 2003;206:1985–92.
[21] Chan DC. Mitochondrial dynamics and its involvement in disease. Annu Rev Pathol 2020;15:235–59.
[22] Chang DT, Reynolds IJ. Mitochondrial trafficking and morphology in healthy and injured neurons. Prog Neurobiol 2006;80:241–68.
[23] Cheah M, Fawcett JW, Andrews MR. Assessment of thermal pain sensation in rats and mice using the Hargreaves test. Bio Protoc 2017;7: e2506.
[24] Chen TW, Wardill TJ, Sun Y, Pulver SR, Renninger SL, Baohan A, Schreiter ER, Kerr RA, Orger MB, Jayaraman V, Looger LL, Svoboda K, Kim DS. Ultrasensitive fluorescent proteins for imaging neuronal activity. Nature 2013;499:295–300.
[25] Chiang H, Ohno N, Hsieh YL, Mahad DJ, Kikuchi S, Komuro H, Hsieh ST, Trapp BD. Mitochondrial fission augments capsaicin-induced axonal degeneration. Acta Neuropathol 2015;129:81–96.
[26] Chiu IM, Barrett LB, Williams EK, Strochlic DE, Lee S, Weyer AD, Lou S, Bryman GS, Roberson DP, Ghasemlou N, Piccoli C, Ahat E, Wang V, Cobos EJ, Stucky CL, Ma Q, Liberles SD, Woolf CJ. Transcriptional profiling at whole population and single cell levels reveals somatosensory neuron molecular diversity. eLife 2014;3:e04660.
[27] Choi S, Na HS, Kim J, Lee J, Lee S, Kim D, Park J, Chen CC, Campbell KP, Shin HS. Attenuated pain responses in mice lacking Ca(V)3.2 T-type channels. Genes Brain Behav 2007;6:425–31.
[28] Choi S, Quan X, Bang S, Yoo H, Kim J, Park J, Park KS, Chung J. Mitochondrial calcium uniporter in Drosophila transfers calcium between the endoplasmic reticulum and mitochondria in oxidative stress-induced cell death. J Biol Chem 2017;292:14473–85.
[29] Chowdhury SK, Smith DR, Fernyhough P. The role of aberrant mitochondrial bioenergetics in diabetic neuropathy. Neurobiol Dis 2013;51:56–65.
[30] Chowdhury SK, Zherebitskaya E, Smith DR, Akude E, Chattopadhyay S, Jolivalt CG, Calcutt NA, Fernyhough P. Mitochondrial respiratory chain dysfunction in dorsal root ganglia of streptozotocin-induced diabetic rats and its correction by insulin treatment. Diabetes 2010;59:1082–91.
[31] Clarke JP, Mearow K. Autophagy inhibition in endogenous and nutrient-deprived conditions reduces dorsal root ganglia neuron survival and neurite growth in vitro. J Neurosci Res 2016;94:653–70.
[32] Coccurello R, Nazio F, Rossi C, De Angelis F, Vacca V, Giacovazzo G, Procacci P, Magnaghi V, Ciavardelli D, Marinelli S. Effects of caloric restriction on neuropathic pain, peripheral nerve degeneration and inflammation in normometabolic and autophagy defective prediabetic Ambra1 mice. PLoS One 2018;13:e0208596.
[33] Coleman MP, Perry VH. Axon pathology in neurological disease: a neglected therapeutic target. Trends Neurosciences 2002;25:532–7.
[34] Court FA, Coleman MP. Mitochondria as a central sensor for axonal degenerative stimuli. Trends Neurosci 2012;35:364–72.
[35] Cribbs JT, Strack S. Reversible phosphorylation of Drp1 by cyclic AMP-dependent protein kinase and calcineurin regulates mitochondrial fission and cell death. EMBO Rep 2007;8:939–44.
[36] daCosta DiBonaventura M, Cappelleri JC, Joshi AV. A longitudinal assessment of painful diabetic peripheral neuropathy on health status, productivity, and health care utilization and cost. Pain Med 2011;12: 118–26.
[37] De Stefani D, Raffaello A, Teardo E, Szabo I, Rizzuto R. A forty-kilodalton protein of the inner membrane is the mitochondrial calcium uniporter. Nature 2011;476:336–40.
[38] Di Marco G, Vallese F, Jourde B, Bergsdorf C, Sturlese M, De Mario A, Techer-Etienne V, Haasen D, Oberhauser B, Schleeger S, Minetti G, Moro S, Rizzuto R, De Stefani D, Fornaro M, Mammucari C. A high-throughput screening identifies MICU1 targeting compounds. Cell Rep 2020;30:2321–31.e2326.
[39] Divisova S, Vlckova E, Srotova I, Kincova S, Skorna M, Dusek L, Dubovy P, Bednarik J. Intraepidermal nerve-fibre density as a biomarker of the course of neuropathy in patients with Type 2 diabetes mellitus. Diabetic Med 2016;33:650–4.
[40] Dyck PJ, Kratz KM, Lehman KA, Karnes JL, Melton LJ III, O'Brien PC, Litchy WJ, Windebank AJ, Smith BE, Low PA, Service FJ, Rizza RA, Zimmerman BR. The Rochester Diabetic Neuropathy Study: design, criteria for types of neuropathy, selection bias, and reproducibility of neuropathic tests. Neurology 1991;41:799–807.
[41] Edwards JL, Quattrini A, Lentz SI, Figueroa-Romero C, Cerri F, Backus C, Hong Y, Feldman EL. Diabetes regulates mitochondrial biogenesis and fission in mouse neurons. Diabetologia 2010;53:160–9.
[42] Elias JE, Gygi SP. Target-decoy search strategy for increased confidence in large-scale protein identifications by mass spectrometry. Nat Methods 2007;4:207–14.
[43] Estacion M, Vohra BP, Liu S, Hoeijmakers J, Faber CG, Merkies IS, Lauria G, Black JA, Waxman SG. Ca2+ toxicity due to reverse Na+/Ca2+ exchange contributes to degeneration of neurites of DRG neurons induced by a neuropathy-associated Nav1.7 mutation. J Neurophysiol 2015;114:1554–64.
[44] Fernyhough P, Calcutt NA. Abnormal calcium homeostasis in peripheral neuropathies. Cell Calcium 2010;47:130–9.
[45] Goswami SC, Mishra SK, Maric D, Kaszas K, Gonnella GL, Clokie SJ, Kominsky HD, Gross JR, Keller JM, Mannes AJ, Hoon MA, Iadarola MJ. Molecular signatures of mouse TRPV1-lineage neurons revealed by RNA-Seq transcriptome analysis. J Pain 2014;15:1338–59.
[46] Granatiero V, De Stefani D, Rizzuto R. Mitochondrial calcium handling in physiology and disease. Adv Exp Med Biol 2017;982:25–47.
[47] Guan L, Che Z, Meng X, Yu Y, Li M, Yu Z, Shi H, Yang D, Yu M. MCU Up-regulation contributes to myocardial ischemia-reperfusion Injury through calpain/OPA-1-mediated mitochondrial fusion/mitophagy Inhibition. J Cell Mol Med 2019;23:7830–43.
[48] Han XJ, Lu YF, Li SA, Kaitsuka T, Sato Y, Tomizawa K, Nairn AC, Takei K, Matsui H, Matsushita M. CaM kinase I alpha-induced phosphorylation

of Drp1 regulates mitochondrial morphology. J Cell Biol 2008;182: 573–85.
[49] He L, Diedrich J, Chu YY, Yates JR III. Extracting accurate precursor information for tandem mass spectra by RawConverter. Anal Chem 2015;87:11361–7.
[50] Huang TJ, Sayers NM, Fernyhough P, Verkhratsky A. Diabetes-induced alterations in calcium homeostasis in sensory neurones of streptozotocin-diabetic rats are restricted to lumbar ganglia and are prevented by neurotrophin-3. Diabetologia 2002;45:560–70.
[51] Jayaraj ND, Bhattacharyya BJ, Belmadani AA, Ren D, Rathwell CA, Hackelberg S, Hopkins BE, Gupta HR, Miller RJ, Menichella DM. Reducing CXCR4-mediated nociceptor hyperexcitability reverses painful diabetic neuropathy. J Clin Invest 2018;128:2205–25.
[52] Kamer KJ, Grabarek Z, Mootha VK. High-affinity cooperative Ca(2+) binding by MICU1-MICU2 serves as an on-off switch for the uniporter. EMBO Rep 2017;18:1397–411.
[53] Kampoli AM, Tousoulis D, Briasoulis A, Latsios G, Papageorgiou N, Stefanadis C. Potential pathogenic inflammatory mechanisms of endothelial dysfunction induced by type 2 diabetes mellitus. Curr Pharm Des 2011;17:4147–58.
[54] Kwong JQ, Lu X, Correll RN, Schwanekamp JA, Vagnozzi RJ, Sargent MA, York AJ, Zhang J, Bers DM, Molkentin JD. The mitochondrial calcium uniporter selectively matches metabolic output to acute contractile stress in the heart. Cell Rep 2015;12:15–22.
[55] Lambert JP, Murray EK, Elrod JW. MCUB and mitochondrial calcium uptake—modeling, function, and therapeutic potential. Expert Opin Ther Targets 2020;24:163–9.
[56] Latremoliere A, Woolf CJ. Central sensitization: a generator of pain hypersensitivity by central neural plasticity. J Pain 2009;10:895–926.
[57] Lauria G, Devigili G. Skin biopsy as a diagnostic tool in peripheral neuropathy. Nat Clin Pract Neurol 2007;3:546–57.
[58] Lauria G, Lombardi R, Camozzi F, Devigili G. Skin biopsy for the diagnosis of peripheral neuropathy. Histopathology 2009;54:273–85.
[59] Lauria G, Morbin M, Lombardi R, Borgna M, Mazzoleni G, Sghirlanzoni A, Pareyson D. Axonal swellings predict the degeneration of epidermal nerve fibers in painful neuropathies. Neurology 2003;61:631–6.
[60] Lehning EJ, Doshi R, Isaksson N, Stys PK, LoPachin RM Jr. Mechanisms of injury-induced calcium entry into peripheral nerve myelinated axons: role of reverse sodium-calcium exchange. J Neurochem 1996;66:493–500.
[61] Li CL, Li KC, Wu D, Chen Y, Luo H, Zhao JR, Wang SS, Sun MM, Lu YJ, Zhong YQ, Hu XY, Hou R, Zhou BB, Bao L, Xiao HS, Zhang X. Somatosensory neuron types identified by high-coverage single-cell RNA-sequencing and functional heterogeneity. Cell Res 2016;26:967.
[62] Lieberman OJ, Choi SJ, Kanter E, Saverchenko A, Frier MD, Fiore GM, Wu M, Kondapalli J, Zampese E, Surmeier DJ, Sulzer D, Mosharov EV. Alpha-synuclein-dependent calcium entry underlies differential sensitivity of cultured SN and VTA dopaminergic neurons to a parkinsonian neurotoxin. eNeuro 2017;4:ENEURO.0167-17.2017.
[63] Ligon LA, Steward O. Movement of mitochondria in the axons and dendrites of cultured hippocampal neurons. J Comp Neurol 2000;427: 340–50.
[64] Loson OC, Song Z, Chen H, Chan DC. Fis1, Mff, MiD49, and MiD51 mediate Drp1 recruitment in mitochondrial fission. Mol Biol Cell 2013;24: 659–67.
[65] Luongo TS, Lambert JP, Yuan A, Zhang X, Gross P, Song J, Shanmughapriya S, Gao E, Jain M, Houser SR, Koch WJ, Cheung JY, Madesh M, Elrod JW. The mitochondrial calcium uniporter matches energetic supply with cardiac workload during stress and modulates permeability transition. Cell Rep 2015;12:23–34.
[66] MacAskill AF, Kittler JT. Control of mitochondrial transport and localization in neurons. Trends Cell Biol 2010;20:102–12.
[67] Mallilankaraman K, Cardenas C, Doonan PJ, Chandramoorthy HC, Irrinki KM, Golenar T, Csordas G, Madireddi P, Yang J, Muller M, Miller R, Kolesar JE, Molgo J, Kaufman B, Hajnoczky G, Foskett JK, Madesh M. MCUR1 is an essential component of mitochondrial Ca2+ uptake that regulates cellular metabolism. Nat Cell Biol 2012;14:1336–43.
[68] Mammucari C, Raffaello A, Vecellio Reane D, Rizzuto R. Molecular structure and pathophysiological roles of the mitochondrial calcium uniporter. Biochim Biophys Acta 2016;1863:2457–64.
[69] Mattson MP, Gleichmann M, Cheng A. Mitochondria in neuroplasticity and neurological disorders. Neuron 2008;60:748–66.
[70] McAlister GC, Nusinow DP, Jedrychowski MP, Wuhr M, Huttlin EL, Erickson BK, Rad R, Haas W, Gygi SP. MultiNotch MS3 enables accurate, sensitive, and multiplexed detection of differential expression across cancer cell line proteomes. Anal Chem 2014;86:7150–8.
[71] Menichella DM, Abdelhak B, Ren D, Shum A, Frietag C, Miller RJ. CXCR4 chemokine receptor signaling mediates pain in diabetic neuropathy. Mol Pain 2014;10:42.
[72] Menichella DM, Jayaraj ND, Wilson HM, Ren D, Flood K, Wang XQ, Shum A, Miller RJ, Paller AS. Ganglioside GM3 synthase depletion reverses neuropathic pain and small fiber neuropathy in diet-induced diabetic mice. Mol Pain 2016;12.
[73] Menke A, Casagrande S, Geiss L, Cowie CC. Prevalence of and trends in diabetes among adults in the United States, 1988-2012. JAMA 2015; 314:1021–9.
[74] Miller RE, Kim YS, Tran PB, Ishihara S, Dong X, Miller RJ, Malfait AM. Visualization of peripheral neuron sensitization in a surgical mouse model of osteoarthritis by in vivo calcium imaging. Arthritis Rheumatol 2018;70:88–97.
[75] Murphy E, Pan X, Nguyen T, Liu J, Holmstrom KM, Finkel T. Unresolved questions from the analysis of mice lacking MCU expression. Biochem Biophys Res Commun 2014;449:384–5.
[76] Obrosova IG, Ilnytska O, Lyzogubov VV, Pavlov IA, Mashtalir N, Nadler JL, Drel VR. High-fat diet induced neuropathy of pre-diabetes and obesity: effects of "healthy" diet and aldose reductase inhibition. Diabetes 2007;56:2598–608.
[77] Orstavik K, Namer B, Schmidt R, Schmelz M, Hilliges M, Weidner C, Carr RW, Handwerker H, Jorum E, Torebjork HE. Abnormal function of C-fibers in patients with diabetic neuropathy. J Neurosci 2006;26: 11287–94.
[78] Otera H, Wang C, Cleland MM, Setoguchi K, Yokota S, Youle RJ, Mihara K. Mff is an essential factor for mitochondrial recruitment of Drp1 during mitochondrial fission in mammalian cells. J Cell Biol 2010;191:1141–58.
[79] Pan X, Liu J, Nguyen T, Liu C, Sun J, Teng Y, Fergusson MM, Rovira II, Allen M, Springer DA, Aponte AM, Gucek M, Balaban RS, Murphy E, Finkel T. The physiological role of mitochondrial calcium revealed by mice lacking the mitochondrial calcium uniporter. Nat Cell Biol 2013;15:1464–72.
[80] Park SK, Aslanian A, McClatchy DB, Han X, Shah H, Singh M, Rauniyar N, Moresco JJ, Pinto AF, Diedrich JK, Delahunty C, Yates JR III. Census 2: isobaric labeling data analysis. Bioinformatics 2014;30:2208–9.
[81] Perocchi F, Gohil VM, Girgis HS, Bao XR, McCombs JE, Palmer AE, Mootha VK. MICU1 encodes a mitochondrial EF hand protein required for Ca(2+) uptake. Nature 2010;467:291–6.
[82] Persson AK, Hoeijmakers JG, Estacion M, Black JA, Waxman SG. Sodium channels, mitochondria, and axonal degeneration in peripheral neuropathy. Trends Molecular Medicine 2016;22:377–90.
[83] Picard M, White K, Turnbull DM. Mitochondrial morphology, topology, and membrane interactions in skeletal muscle: a quantitative three-dimensional electron microscopy study. J Appl Physiol (1985) 2013;114: 161–71.
[84] Pop-Busui R, Boulton AJ, Feldman EL, Bril V, Freeman R, Malik RA, Sosenko JM, Ziegler D. Diabetic neuropathy: a position statement by the American diabetes association. Diabetes Care 2017;40:136–54.
[85] Purwata TE. High TNF-alpha plasma levels and macrophages iNOS and TNF-alpha expression as risk factors for painful diabetic neuropathy. J Pain Res 2011;4:169–75.
[86] Raffaello A, De Stefani D, Sabbadin D, Teardo E, Merli G, Picard A, Checchetto V, Moro S, Szabo I, Rizzuto R. The mitochondrial calcium uniporter is a multimer that can include a dominant-negative pore-forming subunit. EMBO J 2013;32:2362–76.
[87] Rasola A, Bernardi P. The mitochondrial permeability transition pore and its involvement in cell death and in disease pathogenesis. Apoptosis 2007;12:815–33.
[88] Rimessi A, Pozzato C, Carparelli L, Rossi A, Ranucci S, De Fino I, Cigana C, Talarico A, Wieckowski MR, Ribeiro CMP, Trapella C, Rossi G, Cabrini G, Bragonzi A, Pinton P. Pharmacological modulation of mitochondrial calcium uniporter controls lung inflammation in cystic fibrosis. Sci Adv 2020;6:eaax9093.
[89] Roy Chowdhury SK, Smith DR, Saleh A, Schapansky J, Marquez A, Gomes S, Akude E, Morrow D, Calcutt NA, Fernyhough P. Impaired adenosine monophosphate-activated protein kinase signalling in dorsal root ganglia neurons is linked to mitochondrial dysfunction and peripheral neuropathy in diabetes. Brain 2012;135:1751–66.
[90] Rumora AE, LoGrasso G, Haidar JA, Dolkowski JJ, Lentz SI, Feldman EL. Chain length of saturated fatty acids regulates mitochondrial trafficking and function in sensory neurons. J Lipid Res 2019;60:58–70.
[91] Rumora AE, Savelieff MG, Sakowski SA, Feldman EL. Disorders of mitochondrial dynamics in peripheral neuropathy: clues from hereditary neuropathy and diabetes. Int Rev Neurobiol 2019;145:127–76.
[92] Sabouny R, Shutt TE. Reciprocal regulation of mitochondrial fission and fusion. Trends Biochem Sci 2020;45:564–77.
[93] Sancak Y, Markhard AL, Kitami T, Kovacs-Bogdan E, Kamer KJ, Udeshi ND, Carr SA, Chaudhuri D, Clapham DE, Li AA, Calvo SE, Goldberger O,

Mootha VK. EMRE is an essential component of the mitochondrial calcium uniporter complex. Science 2013;342:1379–82.
[94] Serra J, Duan WR, Locke C, Sola R, Liu W, Nothaft W. Effects of a T-type calcium channel blocker, ABT-639, on spontaneous activity in C-nociceptors in patients with painful diabetic neuropathy: a randomized controlled trial. PAIN 2015;156:2175–83.
[95] Shields SD, Ahn HS, Yang Y, Han C, Seal RP, Wood JN, Waxman SG, Dib-Hajj SD. Nav1.8 expression is not restricted to nociceptors in mouse peripheral nervous system. PAIN 2012;153:2017–30.
[96] Shun CT, Chang YC, Wu HP, Hsieh SC, Lin WM, Lin YH, Tai TY, Hsieh ST. Skin denervation in type 2 diabetes: correlations with diabetic duration and functional impairments. Brain 2004;127:1593–605.
[97] Snider WD, McMahon SB. Tackling pain at the source: new ideas about nociceptors. Neuron 1998;20:629–32.
[98] Sommer C, Lauria G. Skin biopsy in the management of peripheral neuropathy. Lancet Neurol 2007;6:632–42.
[99] Spallone V, Lacerenza M, Rossi A, Sicuteri R, Marchettini P. Painful diabetic polyneuropathy: approach to diagnosis and management. Clin J Pain 2012;28:726–43.
[100] Stirling LC, Forlani G, Baker MD, Wood JN, Matthews EA, Dickenson AH, Nassar MA. Nociceptor-specific gene deletion using heterozygous NaV1.8-Cre recombinase mice. PAIN 2005;113:27–36.
[101] Stucky CL, Rossi J, Airaksinen MS, Lewin GR. GFR alpha2/neurturin signalling regulates noxious heat transduction in isolectin B4-binding mouse sensory neurons. J Physiol 2002;545:43–50.
[102] Sullivan KA, Lentz SI, Roberts JL Jr, Feldman EL. Criteria for creating and assessing mouse models of diabetic neuropathy. Curr Drug Targets 2008;9:3–13.
[103] Themistocleous AC, Ramirez JD, Shillo PR, Lees JG, Selvarajah D, Orengo C, Tesfaye S, Rice AS, Bennett DL. The Pain in Neuropathy Study (PiNS): a cross-sectional observational study determining the somatosensory phenotype of painful and painless diabetic neuropathy. PAIN 2016;157:1132–45.
[104] Truini A, Cruccu G. How diagnostic tests help to disentangle the mechanisms underlying neuropathic pain symptoms in painful neuropathies. PAIN 2016;157:S53–9.
[105] Tufi R, Gleeson TP, von Stockum S, Hewitt VL, Lee JJ, Terriente-Felix A, Sanchez-Martinez A, Ziviani E, Whitworth AJ. Comprehensive genetic characterization of mitochondrial Ca(2+) uniporter components reveals their different physiological requirements in vivo. Cell Rep 2019;27:1541–50 e1545.
[106] Uceyler N, Rogausch JP, Toyka KV, Sommer C. Differential expression of cytokines in painful and painless neuropathies. Neurology 2007;69:42–9.
[107] Uceyler N, Vollert J, Broll B, Riediger N, Langjahr M, Saffer N, Schubert AL, Siedler G, Sommer C. Sensory profiles and skin innervation of patients with painful and painless neuropathies. PAIN 2018;159:1867–76.
[108] Usoskin D, Furlan A, Islam S, Abdo H, Lonnerberg P, Lou D, Hjerling-Leffler J, Haeggstrom J, Kharchenko O, Kharchenko PV, Linnarsson S, Ernfors P. Unbiased classification of sensory neuron types by large-scale single-cell RNA sequencing. Nat Neurosci 2015;18:145–53.
[109] Vargas ME, Yamagishi Y, Tessier-Lavigne M, Sagasti A. Live imaging of calcium dynamics during axon degeneration reveals two functionally distinct phases of calcium influx. J Neurosci 2015;35:15026–38.
[110] Vincent AM, Callaghan BC, Smith AL, Feldman EL. Diabetic neuropathy: cellular mechanisms as therapeutic targets. Nat Rev Neurol 2011;7:573–83.
[111] Vincent AM, Edwards JL, McLean LL, Hong Y, Cerri F, Lopez I, Quattrini A, Feldman EL. Mitochondrial biogenesis and fission in axons in cell culture and animal models of diabetic neuropathy. Acta Neuropathol 2010;120:477–89.
[112] Vollert J, Maier C, Attal N, Bennett DLH, Bouhassira D, Enax-Krumova EK, Finnerup NB, Freynhagen R, Gierthmuhlen J, Haanpaa M, Hansson P, Hullemann P, Jensen TS, Magerl W, Ramirez JD, Rice ASC, Schuh-Hofer S, Segerdahl M, Serra J, Shillo PR, Sindrup S, Tesfaye S, Themistocleous AC, Tolle TR, Treede RD, Baron R. Stratifying patients with peripheral neuropathic pain based on sensory profiles: algorithm and sample size recommendations. PAIN 2017;158:1446–55.
[113] von Hehn CA, Baron R, Woolf CJ. Deconstructing the neuropathic pain phenotype to reveal neural mechanisms. Neuron 2012;73:638–52.
[114] Wainger BJ, Kiskinis E, Mellin C, Wiskow O, Han SS, Sandoe J, Perez NP, Williams LA, Lee S, Boulting G, Berry JD, Brown RH Jr, Cudkowicz ME, Bean BP, Eggan K, Woolf CJ. Intrinsic membrane hyperexcitability of amyotrophic lateral sclerosis patient-derived motor neurons. Cell Rep 2014;7:1–11.
[115] Wang JT, Medress ZA, Barres BA. Axon degeneration: molecular mechanisms of a self-destruction pathway. J Cel Biol 2012;196:7–18.
[116] Wiemerslage L, Lee D. Quantification of mitochondrial morphology in neurites of dopaminergic neurons using multiple parameters. J Neurosci Methods 2016;262:56–65.
[117] Woods JJ, Nemani N, Shanmughapriya S, Kumar A, Zhang M, Nathan SR, Thomas M, Carvalho E, Ramachandran K, Srikantan S, Stathopulos PB, Wilson JJ, Madesh M. A selective and cell-permeable mitochondrial calcium uniporter (MCU) inhibitor preserves mitochondrial bioenergetics after hypoxia/reoxygenation injury. ACS Cent Sci 2019;5:153–66.
[118] Xu S, Chisholm ADC. Elegans epidermal wounding induces a mitochondrial ROS burst that promotes wound repair. Dev Cell 2014;31:48–60.
[119] Zhang JM, Song XJ, LaMotte RH. Enhanced excitability of sensory neurons in rats with cutaneous hyperalgesia produced by chronic compression of the dorsal root ganglion. J Neurophysiol 1999;82:3359–66.
[120] Zhao L, Li S, Wang S, Yu N, Liu J. The effect of mitochondrial calcium uniporter on mitochondrial fission in hippocampus cells ischemia/reperfusion injury. Biochem Biophys Res Commun 2015;461:537–42.
[121] Zimmet PZ, Magliano DJ, Herman WH, Shaw JE. Diabetes: a 21st century challenge. Lancet Diabetes Endocrinol 2014;2:56–64.